North Carolina Agricultural and Technical State University

Aggie Digital Collections and Scholarship

2014

Processing And Modeling Of Porous Copper Using Sintering Dissolution Process

Mustafa Abualgasim Salih
North Carolina Agricultural and Technical State University

Follow this and additional works at: https://digital.library.ncat.edu/theses

Processing and Modeling of
Porous Copper Using Sintering Dissolution Process

Mustafa Abualgasim Abdalhakam Salih

North Carolina A&T State University

A thesis submitted to the graduate faculty

in partial fulfillment of the requirements for the degree of

MASTER OF SCIENCE

Department: Mechanical Engineering

Major: Mechanical Engineering

Major Professor: Dr. Cindy Waters

Greensboro, North Carolina

2014

The Graduate School
North Carolina Agricultural and Technical State University
This is to certify that the Master's Thesis of

Mustafa Abualgasim Abdalhakam Salih

has met the thesis requirements of
North Carolina Agricultural and Technical State University

Greensboro, North Carolina
2014

Approved by:

_____

Dr. Cindy Waters   Dr. Trisha Sain
Major Professor   Committee Member

Dr. John Kizito   Dr. Samuel Owusu-Ofori
Committee Member   Department Chair

Dr. Sanjiv Sarin
Dean, The Graduate School

Biographical Sketch

Mustafa A. Salih was born in March 1984 in Jayzan, Saudi Arabia. He earned his Bachelor of Mechanical Engineering in 2007 from Sudan University of Science and Technology. He is presently in his last semester of study in the Mechanical Engineering and he will graduate with a Master of Science degree in Mechanical Engineering Department at North Carolina A&T State University.

Acknowledgements

First, above all I thank Allah whom I believe is the ultimate guide for enabling me to finish the project and my life in general.

I would like to express my deepest gratitude to my supervisor Dr. Cindy for her continuous encouragement, valuable advice and unlimited support, even for personal matters. Without their help and guidance this thesis would not has come out as it did.

I would also like to thank my committee members; Dr. John Kizito and Dr. Trisha Sain Special thanks to the whole research team of the department especially Stephen Ajinola and Ahmadreza Sedighi for their help and support. I am thankful my friends and colleagues; Sabri Abdelwahab, Ali Osman and Sanad Almahal for their help and patience. Additional thanks go to various friends for their support and encouragement.

An extension of my gratitude is also given to Dr. Boyce Collins and John Skujins who assisted me throughout my research work. In addition valuable support was provided from the Center for Composite Materials Research and the National Science Foundation Award # 0959511: "MRI-R^2: Acquisition of a Nanotom Computed Tomography System for Revolutionizing Metallic Biomaterials Research, Education, and Training.

No word could express my gratitude to my parents and siblings; Mohamed, Ahmed and Alamin who have been consistently supporting me with their well and for their unflagging love, encouragement and support throughout my life.

Thank you so much!

Mustafa A. Salih

Table of Contents

List of Figures

List of Tables

Abstract

The growth of porous metal has produced materials with improved properties as compared to non-metals and solid metals. Porous metal can be classified as either open cell or closed cell. Open cell allows a fluid media to pass through it. Closed cell is made up of adjacent sealed pores with shared cell walls. Metal foams offer higher strength to weight ratios, increased impact energy absorption, and a greater tolerance to high temperatures and adverse environmental conditions when compared to bulk materials. Copper and its alloys are examples of these, well known for high strength and good mechanical, thermal and electrical properties.

In the present study, the porous Cu was made by a powder metallurgy process, using three different space holders, sodium chloride, sodium carbonate and potassium carbonate. Several different samples have been produced, using different ratios of volume fraction. The densities of the porous metals have been measured and compared to the theoretical density calculated using an equation developed for these foams. The porous structure was determined with the removal of spacer materials through sintering process. The sintering process of each spacer material depends on the melting point of the spacer material.

Processing, characterization, and mechanical properties were completed. These tests include density measurements, compression tests, computed tomography (CT) and scanning electron microscopy (SEM). The captured morphological images are utilized to generate the object-oriented finite element (OOF) analysis for the porous copper. Porous copper was formed with porosities in the range of 40-66% with density ranges from 3 to 5.2 g/cm³. A study of two different methods to measure porosity was completed.

OOF (Object Oriented Finite Elements) is a desktop software application for studying the relationship between the microstructure of a material and its overall mechanical, dielectric, or

thermal properties using finite element models based on real or simulated micrographs. OOF provides methods for segmenting images, creating meshes and solving of complex geometries using finite element models, and visualizing 2D results.

CHAPTER 1

Introduction

Metallic foam and porous metals are gaining wide interest in a variety of fields. Both are permeable for gaseous and liquid media but they have different manufacturing technologies and therefore different properties. The distinguishing factor of metal porous is a very high porosity; usually 75–95% of the volume consists of void spaces. Many restrict usage of the word "solid foam" to mean materials which were created from the liquid state. The literature contains a wide berth of publications that also call porous structures such as sintered metal powders "foams" although they were not created from the liquid state (J. Banhart & Baumeister, 1999). Fraunhofer- Institute for Applied Materials Research (IFAM)) Subsequently, this work will use the standard that foams are formed from a liquid state process and porous metals come from a powder metallurgy route. Metal powders can be cast together with crystal salt into the desired shape before the salt is washed out and thus salt grain pores replace their contact points, same porous metals are also called cellular materials containing interconnected pores.

Metal foam fabrication started in the 1940s by Sosnik with one of the first products being aluminum foam. However, after seven decades metal foams are still considered a new class of materials (Mansourighasri, Muhamad, & Sulong, 2012).

The development of these structures improves the properties when compared to solid metal and non- porous metal. In comparison, porous metal offer higher specific stiffness (stiffness to weight ratio) and mechanical properties can be engineered to meet the demands of a wide range of applications by changing the size, shape, and volume fraction of cells. Compared to non-porous metal, porous metal offer higher stiffness, better strength to weight ratios, increased impact energy absorption, a greater tolerance to high temperatures, and greater

tolerance to adverse environmental conditions.

Porous metals are open cell, closed cell, or a mixture of the two. They from a network of consistent solid struts it allows fluid media to pass through it. The open-cell porous has the cell edges connected and leaves open the cell faces (Shih & Huang, 2006). Closed cell porous is made up of a network of adjacent sealed pores, all sharing walls with each other. The closed-cell structure is consisted of cell faces and edges so that each cell is sealed off from its neighbor (Castro, 2013). The difference between the open and closed cell is clearly seen in pores. Open cell allows the passage of fluids and gasses for different applications ranging from filtering to heat exchange and gives the porous its increased surface area while the closed cell arrangement is better for energy absorption and structural applications such as car bumpers, bridges and buildings (A. K. Shaik Dawood, 2010).

1.1 Applications of Porous Metals

Porous metals can be distinguished by their applications. Some applications need to optimize weight and therefore exploit their lightweight nature and other applications utilize porous metals unique structure.

1.1.1 Weight optimizing applications. In the field of porous metal, porous have been creating particular interest owing to their lightweight structure and good physical, chemical and mechanical properties, which make them suitable for a range of industrial applications.

1.1.1.1 Automotive industry. The rising request for safety of automobiles has led to a higher vehicle weight in many cases. This conflicts with further demands for low fuel consumption, necessitating additional measures for weight reduction. A car with parts made of aluminum foam and a muffler component using metal foam shown in Figure 1.
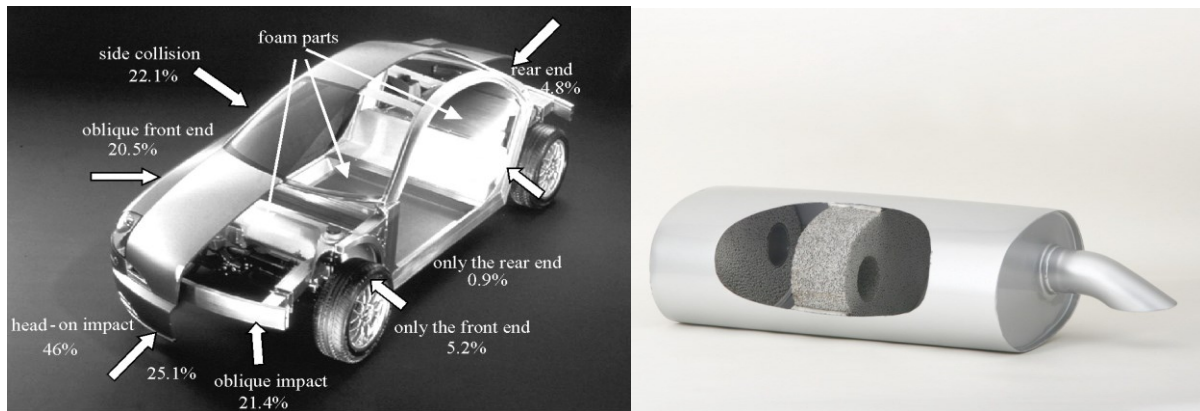
*Figure 1. (*a) A car with parts made of aluminum foam. (b) Cut by a muffler component using metal foam (C. A. Andreas Ochsner, 2009)

The good relation between weight and stiffness supports the use porous metals in large area light-weighting automobile body sheets and structural parts that are used in the area of the automotive with increased requirements on the stability. Examples are trunk lids, engine hoods and sliding roofs. In view of background the good energy and sound absorbing properties of the porous metal especially porous aluminum support the use in passenger cars, this application is illustrated in the case of crash-absorbers against side and front impact (Catrin Kammer, 1999). There are three main applications of porous metal could made them more important in automotive:

- Light-weight construction

- Crash energy absorption

- Noise control

1.1.1.2 Aerospace industry.   In aerospace applications, the replacement of expensive honeycomb structures by porous metal or aluminum sheets sandwich panels could led to higher performance at mechanical and thermal properties. Porous metals use in structural parts in turbines where the enhanced stiffness in conjunction with increased damping is valuable, seals

between the various stages of the engine are similarly made of porous metals. The turbine blade cuts the desired contour into the cellular material in its first operation and creates an almost gas-tight seal this way. Porous aluminum has been evaluated for its use also an energy absorbing crash element for space vehicle landing pads and as reinforcement for load bearing structures in satellites, replacing materials that cause problems in the adverse environmental conditions in space (John Banhart, 2001).

1.1.1.3 Biomedical industry. Porous metal have been initially proposed at the end of the 1960's to overcome problems encountered with bone cement. The goal was to produce a rough surface that increases the friction forces between the implant and the surrounding bone thus providing better initial stability to the implant. After implantation, the bone grows into the porous surface and helps to secure the long-term stability of the implant (Lefebvre, Banhart, & Dunand, 2008).

Titanium and cobalt–chromium foam are used for prostheses and dental implants because of their biocompatibility. To certify ingrowth of tissue, one usually produces a porous layer of the same or another biocompatible material on the prosthesis by thermal spraying or other methods. Otherwise, one could use porous titanium or titanium foam for many applications and modify the density distribution to meet the requirements concerning strength, moduli, etc. of components.

Magnesium foams could be used as recyclable implants that serve as load bearing structure as long as the bone still grows but are gradually absorbed by the body in a later stage of convalescence (Thabarealam, 2009).

Porous tantalum foam structures are used as bone growth models. It has been considered for many years to be biocompatible as a result of the stable tantalum oxide (Ta_2O_5) that forms on

its surface. Ta and sponges are more mechanically stable comparatively to mesh structures; they are still limited due to the open spaces present throughout the scaffold (Narayan & SpringerLink, 2009).

1.1.1.4 Shipbuilding. In ships the necessity for lightweight materials is very significant. And also a high flexibility of materials processing is needed. Thus porous metal especially aluminum foams can have great advantages. Essential for the use will the development of suitable fastening elements and the examination of corrosion of aluminum foams in salt water. A sodium chloride solution could enter only the uppermost layer of the foam without causing structural defects (Catrin Kammer, 1999).

1.1.1.5 Machine construction. There are some beautiful applications for metallic foams in machine construction. Stiff foamed parts or foam-filled columns with reduced inertia and enhanced damping could replace axles, rolls or platforms currently made of conventional metal. Some components can be used in stationary drilling or milling machines, as well as in printing machines. Housings for small hand-held drilling or grinding machines offer some advantages over traditional housings such as an enhanced intrinsic damping.

1.1.2 Functional applications. The major application in this field contains heat exchangers, filtration and separation, water purification, cooling machines, acoustic control, silencers and flame arresters. In industrial application increasing in demand has led to the growth of the powder metallurgy, which has created porous sintered metals for many applications (Thabarealam, 2009).

1.1.2.1 Heat exchangers and cooling machines. One of the most important classes of porous media is porous metal with low density and novel thermal, mechanical, electrical, and acoustic properties. Having high surface to volume ratio, being lightweight with high strength

and rigidity, it can be used in thermal applications as highly efficient heat exchangers and in addition to existing porous matrix heat exchangers (Ejlali, Ejlali, Hooman, & Gurgenci, 2009).

In porous metal heat exchangers, heat is conducted through metallic ligaments, which have a large accessible surface area per unit volume, and acts as turbulence generator for downstream ligaments, resulting in high interfacial convection heat transfer (Tamayol & Hooman, 2011).

The applications of heat exchangers porous metal having high thermal conductivity such as copper and aluminum porous are needed and some of the recent applications are open cellular materials in transpiration cooling in which properties like high surface area, low flow resistivity and good thermal conductivity plays a significant functions (Thabarealam, 2009).

1.1.2.2 Filtration and Separation. Filtration is one of the separation processes where solid materials are removed from a gas or liquid with minimum pressure drop. The depth filter has some special characteristics meanwhile the porous material has the depth filtration medium with nominal pore size and length of passage qualities, which can absorb dirt called dirt holding and it also possess high pressure and temperature absorbing capacity. Outstanding to its high permeability in nature it becomes clearly metal for filtering gases, acids and other liquids. The good corrosion resistance and high mechanical strength properties of titanium gives a vital role in strong environment reactions and rise to long life plus clean ability (Thabarealam, 2009).

1.1.2.3 Electromagnetic shielding. Porous metals have a high stiffness to mass ratio, thus it is well suited for building lightweight structures that can bear loads while their deformation remains small. It also has the additional useful functionality that it shields electromagnetic waves very well.

Porous metals available in this field are mainly the three-dimensional reticulated copper or nickel with the internal cells all interconnected one another (Wang, See, Ling, & Koh, 2012). Mobile telephone nets rely on a large number of wireless relay stations and transmitters placed on high masts. Such transmitters have to be shielded electromagnetically in order to avoid an adverse effect of the radiated electromagnetic pulses on the electronics and computers of the relay stations. In addition, the shielding has to bear forces by strong winds and have a good electrical conductivity around the entire circumference (J. Banhart, 2009).

1.1.2.4 Silencer. Components for dampening of sound, pressure pulses and mechanical vibrations used in industrial applications of powder metallurgy (John Banhart, 2001) which is also a common used in industrial application of parts manufactured by powder metallurgy. These porous materials can be utilized in dampening of sound at many frequencies. Sudden pressure changes occurring in compressors or pneumatic devices can be damped with porous sintered elements (Duarte & Banhart, 2000).

1.2.2.5 Impact Energy Absorption. The porous materials are able to absorb a significant amount of impact energy through their elastic and plastic deformation during the loading process. Figure 2 shows force-displacement and stress-strain curve of general porous metal which is represented by the area under the strain-stress curve Ideal energy absorbers have a long and flat stress-strain curve, which depends on the base material, relative density and the strain rate. With a proper choice of material foam design parameters, its response can be easily adjusted to certain application demands.
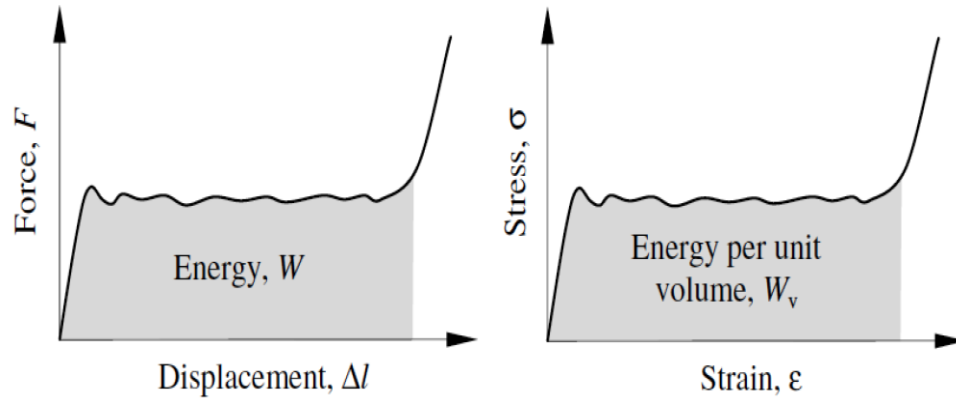
Figure 2. Force-displacement and stress-strain curve of general porous metal (C. A. Andreas Ochsner, 2009)

Some other functional applications of porous metals are listed bellow:

• Flame and sparkle arresters

• Supports for catalysts

• Fluid flow control

• Acoustic control and sound absorber

• Electrochemical applications

1.2 Production Methods

There are a large variety of methods to produce porous metals or similar structures by using liquid metal, powdered metal and an electrolyte containing metal ions. Each process works for a selection of metals or alloys and yields foams of a typical morphology and density range.

1.2.1 Foaming of liquid metals. Creating gas bubbles in a liquid metal can form porous metals. This can be done by adding fine ceramic powders or alloying elements to the melt that form stabilizing particles, or by other means (N. Babcsán 2003).

Presently three ways for foaming metallic melts are identified; firstly, by injecting gas into the liquid metal, second, causing the precipitation of gas which was previously dissolved in

the liquid, third, by causing an in-situ gas release in the liquid by admixing gas-releasing blowing agents to the molten metal.

   1.2.2 Foaming metallic precursors. Another class of metal foaming techniques adds an additional step to the process chain. Instead of foaming the melt directly, a precursor is prepared which contains a uniformly dispersed blowing agent. The foam is created in a second step by melting the precursor during which the blowing gas evolves and bubbles are created. The advantage of this process is that complex shaped parts can be manufactured by filling molds with the precursor and foaming. Metal foam precursors have been prepared in three ways (N. Babcsán 2003)

- By densifying mixtures of powders containing a blowing agent in the solid state

- By shaping such powder blends by thixo-casting in the semi-solid state and

- By admixing blowing agent powders to melts which are then solidified.

1.3 Challenges for Porous Materials

   A major concern with the use of porous implants in highly loaded applications is the effect the porous matrix might have on fatigue strength. Ti alloys and Co–Cr alloys have experience drastic reductions in fatigue strengths when fabricated as porous coatings on solid core structures. Reports have been shown that the high cycle fatigue strength of porous coated Ti alloy is approximately one-third that of the solid alloy equivalent shape, probably even less in fully porous matrices (Ryan, Pandit, & Apatsidis, 2006).

   Mechanical properties of porous materials can be improved and optimized by controlling porosity, pore size and shape as well as pore distribution (Jacobs, Gilbert, & Urban, 1998). Corrosion can also affect ultimate strength of the material, limit the fatigue life and lead to the mechanical failure of the implant. There is a low but finite prevalence of corrosion related

fracture of implants. Increased surface areas, in porous implants, have shown higher corrosion rates when tested in vitro compared to conventional non porous-coated implants. In summary problems arise with using porous metals

- Porous metals are still too expensive: Mass production will lead to lower prices but metal foam will never be a really cheap material.

- Lack of understanding of the basic mechanisms of metal foaming: Knowledge is still speculative and some points remain unclear. Example, what is the reason for the existence of a critical cell wall thickness?

- The interrelationship between morphology and structure on the one hand, and mechanical (or other) properties on the other is not sufficiently understood,

- Insufficient ability to make foams of a constant quality with predefined parameters, which is the lack of control of structure and morphology.

- Physical properties of foams are not good enough: There looks to be still some potential for an improvement of properties by optimizing foaming processes and materials selection.

CHAPTER 2

Literature Review

Porous metals with their traditional classifications (closed and open cell) have been attracted by many industrial applications as their manufacturing methods and develop rashly. Among those applications, porous electrodes in rechargeable batteries, fuel cell, electric composition, electrochemical catalysis, heat exchangers, filter and some other electrochemical processes like chlorine and chlorine by-products production, nitrites removal, and water electrolysis. Porous copper is characterized by a highly porous cell structure. Their large ductility as well as good thermal and electrical conductivity makes them very attractive for such industrial applications (Shehata Aly, Almajid, Nakano, & Ochiai, 2009).

2.1 Porous Copper Properties and Applications

The porous copper has many applications in the modern society due to its excellent thermal conductivity, electric properties, resistance to the corrosion, and resistance to the fatigue and good mechanical properties. Connectors, contact switches, heaters, valves, piping, pots for absorption of solar energy, radiators for automobiles, current driver, electronic driver, contact sheets, elements of thermostats are common applications. Copper can be used with high purity or with addition of alloy elements (Ni, Sn, Be, Pt, Cr, Nb, Pb, Al) that increase the principal properties.

Products based on copper alloys such as porous material filters, electric friction equipment, contacts and structural parts can be manufactured through the process of powder metallurgy, which have the advantages of making fine grained homogeneous structures, forming complicated shapes with close dimensional tolerances and the ability to produce parts with a superior surface finishing. These advantages reduce or eliminate costly machining processes and

allow less scrap loss, compared to other forming methods.

2.2 Metallurgy Techniques

The fabrication of porous metal implants can be divided into three categories, classified according to the state the metal is processed in:

- Liquid metal,

- Solid state in powdered or fiber form,

- Metal vapor or gaseous metallic compounds (Ryan et al., 2006).

2.2.1 Powder metallurgy techniques. The powder metallurgy route is an attractive method for producing porous metals. This technology brings a significant reduction in costs in comparison to earlier applied galvanic methods and all materials suitable for sintering can be applied (S. M. Andreas Ochsner, Hossein Hosseini, Markus Merkel, 2010).

The main disadvantages of powder metallurgy techniques are their relatively high cost, due mainly to the handle fine metal powders. However it different from others powder techniques, the Sintering and Dissolution Process does not require an expensive powder foaming agent but only a culinary salt with saving of money and protections (Surace, De Filippis, Ludovico, & Boghetich, 2009).

The high melting temperature and strong chemical reactivity of titanium united with high affinity of the melt to atmosphere and high melt reactivity with conventional mold materials makes melt based foaming techniques unviable. Among other potential technologies, the powder metallurgy based -space holder technique- in which a sacrificial material such as carbamide, magnesium or sodium chloride and other is used as space holder, is reported extensively. The technique consists of mixing the granular space holder with metal powder, compaction of the powder mixture, leaching of space holder material to leave high volume fraction of porosity and

then sintering to reduce secondary porosity and impart good mechanical properties. This technique involves conventional equipment relatively low sintering temperature for Ti foam, and high porosity of final products (Smorygo et al., 2012).

The easiest way of achieving desired porosity levels using powder metallurgy is by low pressure compaction and a partial sintering technique, in which the pore shape, size and amount are determined by the shape, size and amount of the powder particles (Esen & Bor, 2007).

The difference between liquid metallurgy technique and powder metallurgy technique is, liquid metallurgy method involves foaming of metallic melt either by using reactant and foaming agent, or by inert gas injection in the melt. The foaming agent and the reactant are mixed after pretreatment into the melt through mechanical stirrer; and are allowed to dissociate the foaming agent to release gases so that the metallic foam is formed. Powder metallurgy powder route involves metal and foaming agent, which are mixed and compacted. Then the compacted mass is heated just above the solidus temperature under pressure. The powder compaction of metal and foaming agent can be subsequently hot rolled to obtain sheet of porous metallic foam (A. K. Shaik Dawood, 2010).

2.3 Properties of Porous Metals

The basic objective behind this developmental process is the unique combination of physical and mechanical properties expected from metallic porous such as high stiffness, low specific weight, high gas permeability, low thermal conductivity, unusual acoustic properties, high impact absorption capacity, and good electrical insulating properties.

2.3.1 Mechanical properties. The main studies on porous metals are on their mechanical properties, where the large application involved in this platform that is primarily known as load bearing. The porous materials in general have fewer functions in the field of

mechanical structures as compared to the functional properties such as acoustic, surface area. But, these porous metals require minimal mechanical properties to avoid failure or damage (Thabarealam, 2009).

The strength of porous metals made by powder sintering depends not only on the amount of porosity and the power material identity, but also equally on the particle size and the sintering temperature and time. Strength decreases faster than expected based on the volume fraction of the solid phase. The reason is that mechanical properties are highly sensitive to pore shape. Pore edges act as stress concentrators, reducing strength and especially plasticity. The greater the number and area of particle contacts, the better the mechanical properties of a sintered metal (Shapovalov, 2002).

2.3.2 Thermal properties. Thermal properties are significant properties for the porous metals to become more attractive along with the combination of conductive, permeable and high surface area for various applications like heat exchangers, heat sink, heat pipes (Lefebvre et al., 2008).

Heat transmission in porous materials may happen by solid conduction, convection, and radiation. In sintered porous metals, solid contact conduction leads, although at high temperatures the contribution of radiation becomes substantial. Convection is of secondary importance here; so sintered porous materials always have lower conductivities than similar pore fewer metals (Shapovalov, 2002).

The efficiency of heat exchange is affected by the conductivity of porous metals, heat exchange between the porous and surrounding fluid and pressure drop. The major characteristics are affected by various structural parameters like pore size distribution, density, cell connectivity and surface roughness, which are complicated to measure and integrate.

2.3.3 Permeability. Permeability is based on the study of a gas or liquid flow through a porous medium. Permeability is one of the major properties in case of porous materials that allow water; acids to flow through the porous metals used in the major application such as porous implants thermal absorption and filtration (Mostafid, 2007).

Permeability, which can be considered as the rate at which a viscous fluid flows through a porous medium is described by Darcy's law where is the first mathematical model of the pressure drop (Δp) of a porous medium of a length (L) and a permeability (k) to the flow velocity (U) in a porous medium based on experimental observations (Singh et al., 2009)

$$\frac{\Delta p}{L} = \frac{\mu}{k} U \ldots \ldots \ldots \ldots \ldots \ldots \ldots (1)$$

Flow resistance is one of the important factors in permeability, where lower the resistance, lesser the energy flow through the porous metals, high resistance can allow desirable transition in reactant mass transport mode in fuel cells (Thabarealam, 2009). This characteristic is very sensitive to the pore space topology. Porous metals are more convenient than polymer foams as they are weak and subject to deform as they traversed by the fluid flow. Pressure drag generally declines as the amount of porosity is increased. However, a material with less tortuous pores will be more permeable.

2.3.4 Electrical conductivity. As the porosity is increased, the electrical conductivity of a porous metal declines in a unequal manner similar to that of the thermal conductivity This decrease is due to the imperfect nature of particle contacts where energy of electrons is dissipated. The reduction in the electric conductivity is almost strictly proportional to an increase in the amount of porosity (Shapovalov, 2002).

2.3.5 Acoustic properties. The porous metals have the unique structure that is well suited for the sound absorbers. Porous metals are commonly considered to be the good sound

absorbers that are mainly used in acoustic applications. Nevertheless, the acoustic properties of porous metals are much less than the polymers foams, so it overtake the opportunities in the field of engineering along with their related mechanical and thermal properties (Thabarealam, 2009).

2.4 Characterization of Porous Metals

Porous metals are characterized by different methods to find the mechanical or physical properties or to evaluate the technological applicability. Several production methods result in characteristic structures, densities and likewise imperfections. The most important parameters to characterize a porous metal are the morphology of the cell (cell geometry, open or closed cell), the topology, the relative density, the mean cell size, its distribution, the properties of the cell wall material mechanical properties and corrosion behavior of the metal foams.

2.5 Sintering

There is no single definition of sintering that covers all of its theoretical and practical aspects and takes into account the various stages involved. It may be defined as "a thermal treatment for bonding particles together into a coherent, predominantly solid structure via mass transport events that occur largely at the atomic level. The bonding leads to improved strength and a lower system energy (German, 1996).

Sintering can also be defined as "heat treatment of a powder mass or a porous compact in order to change their properties toward the properties of the pore-free body." In a powder mass, there is some excess energy due to the large free surface of the powder. This is not a large amount and is insufficient to drive the sintering process by itself. For most powders in powder metallurgy, the sintering stress ranges from 0.04 to 4MPa, which are roughly the same size as those encountered underwater in a swimming pool (German, 1998).

Sintering occurs when powder particles are heated up to about 80% of their melting

temperature. This process step is carried out in vacuum or inert gas to avoid surface reactions of the metal powder. Such surface reactions as oxidation may make the sintering process impossible by inhibiting the surface diffusion, the basic mechanism responsible for sintering.

An additional production process is with the use of an industrial hydraulic molding press. This press shapes the spheres into a component like form. So the metal binder holdup on the core interconnects with its neighboring coated spheres. The advantage of this method is that the joints between the spheres exhibit the same characteristics as the spheres themselves, so this is best used for high temperature applications (C. A. Andreas Ochsner, 2009).

2.6 Basic Mechanisms of Sintering

2.6.1 Solid state sintering of homogeneous material. Judging by the changing shape of the interspace between sintering particles, the sintering process passes through two different stages:

- An early stage with local bonding between adjacent particles, and

- Late stages with pore rounding and pore shrinkage.

Bonding between powder particles requires transport of material from their inside to points and areas where they are in contact with one another. Pore rounding and pore shrinkage require transport of material from the dense volume to the pore surfaces, as well as from softer to sharper corners of the pore surface. In the absence of a liquid phase, five different transport mechanisms are possible:

- Volume diffusion (migration of vacancies),

- Grain-boundary diffusion,

- Surface diffusion,

- Viscous or plastic flow (caused by surface tension or internal stresses),

- Evaporation/condensation of atoms on surfaces (da Costa, da Silva, Ambrozio Filho, & Gomes, 2008).

2.6.2 Solid state sintering of heterogeneous material. Solid state sintering is a thermal process that occurs at temperatures where is the melting point of the powder material. The driving force for binding is a physical diffusion of metal atoms from one particle to another. This is inherently a slow phenomenon and illustrates the main drawback of solid state sintering. (Schueren & Kruth, 1995). When a mixture of particles of two different metals is being sintered, alloying takes place at locations where necks are formed between particles of different metallic identity. These two processes interact with one another However, the growth rate of the neck now depends not only on the diffusion rates in the two pure metals but also on the different diffusion rates in the various alloy phases being formed in and on either side of the neck. On the other hand, the neck width controls the rate of alloy formation. (Ivensen, 1973)

2.6.3 Sintering in presence of a transient liquid phase. Liquid phase sintering (LPS) is a much faster sinter/densification mechanism. The basic material here consists of a mixture of two metal powders: a high melting point metal, called the structural metal, and a low melting point metal, called the binder. Applying heat to the system causes the binder to melt and flow into the porosities formed by the non-molten particles (Schueren & Kruth, 1995).

Consider a compact made from a mixture of particles of two different metals. If one component of the mixture melts at sintering temperature, the arising liquid phase is first being pulled by capillary forces into the narrow gaps between the particles of the solid component, creating the largest possible contact area between liquid and solid phase. Then, alloying takes place and, if the initial proportion of the liquid phase is smaller than its solubility in the solid phase, the liquid phase eventually disappears. The bulk volume of the compact swells because

the melting particles leave behind large pores, while the framework of solid particles increases in volume corresponding to the amount of dissolved liquid phase (Ivensen, 1973).

2.7 Open Cell and Close Cell Foam

Open-cell foams are being used for various purposes such as filters and carriers for catalysts and bioreactors. Filters made from open cell foams with controlled pore sizes can be used for filtration of high temperature gas and fluid.

Open pores have more applications than closed pores. It also has lower density and higher specific surface area than solid materials. These changes in the properties of solid materials due to the pores lead to different applications. However, an increase in porosity lowers the mechanical strength of the material and therefore limits the practical capabilities of these materials. For some operating conditions by using porous materials, using porous materials needs both open-cell and high strength foams (Kashef et al., 2011).

Open cell metallic foam typically achieves mechanical properties close to theoretical predictions. While the mechanical properties of closed cell metallic foams theoretically exceed those of open cell foams, in practice, defects, in the form of elliptical cells or curved cell walls, reduce their measured properties to values similar to those for open-cell foams (W.S. Sanders, 2003). Open cellular are being utilized in orthopedic and dentistry implants such as titanium due to their excellent mechanical properties and biocompatibility. Closed cell metallic foams possess higher modulus, strength and impact energy absorbing characteristics. It may be mentioned that titanium foams are difficult to process through liquid metallurgy route due to the high melting point and chemical reactivity of the element with atmospheric gases (Sharma, Gupta, Modi, Prasad, & Gupta, 2011).

A main classification of porous metals, or metal foams, is between open-cell and closed-cell. In closed-cell foams all cell is completely enclosed by a thin wall or membrane of metal, at the same time as in open-cell foams the individual cells are interconnected, allowing tissue to infiltrate the foam and anchor it into position. Closed-cell porous metals are usually the result of an arbitrary foaming process, in which the size, shape and location of pores within the matrix varies, depending on the parameters of the fabrication process (Ryan et al., 2006).

2.8 Object Oriented Finite Element Simulation

The object-oriented finite element model OOF, developed at the Center for Computational and Theoretical Materials Science (CTCMS) at US National Institute of Standards and Technology (NIST) (http://www.ctcms.nist.gov/oof/oof2/). This method enables complex two-dimensional microstructures to be modeled using images of the actual microstructures. It is a new finite element model technique that can be used to determine macroscopic properties from images of real microstructures. It is becoming an increasingly popular tool for the computation of properties like thermal conductivity and elastic modulus of multi-phase materials with complex microstructures. OOF can be used to determine various properties of a structure, and it is important to know what it is that is desired (Bakshi, Bhargava, Mohammadizadeh, Agarwal, & Tsukanov, 2011).

Although OOF is temporarily limited to elasticity and thermal conductivity calculations in two dimensional microstructures, it has given very promising results in analyzing stress transfer and fracture mechanisms, crack propagation and thermal conductivity of heterogeneous materials (Dong, Bhattacharyya, & Hunter, 2008). In the first step several micrographs were taken from randomly selected positions. Next, the image files were converted to ppm. By setting a threshold value for the pixel brightness, the pixels were divided into two groups, matrix

(white) and pores (black). Setting a correct threshold value is a critical step in image processing, and has been extensively examined in the context of porosity evaluation. Examined the variability in the porosity measured using an image analysis program by analyzing a group of 60 grayscale SEM micrographs of a YSZ coating at different magnifications. The standard deviation in the measured porosity due to all factors (threshold setting, magnification, and area to area difference in actual porosity) was 5% (Azarmi, Coyle, & Mostaghimi, 2009).

The adaptive mesh (skeleton) option facilitates discretization of image such that it confines the pixel boundary. The confirmation to microstructure boundary is controlled by the two properties:

(i)   Homogeneity and

(ii)   Shape of the element.

These two important properties have been quantified by the term 'energy'. The homogeneity energy represents degree of pixel boundary confirmation by mesh elements. The shape energy quantifies the shape quality of the element. These two energy measures have been combined by the factor α that allows the control of relative weight of homogeneity and shape of the mesh.

The optimum homogeneity and shape of the elements can be achieved by performing some strategic sequence of skeleton modification operations. The most challenging operational step is to generate the mesh that conforms to the microstructural boundary. It is also a critical step from the finite element point of view since the accuracy of finite element solution depends on this homogeneity and quality of finite element mesh. Once the mesh is generated, boundary conditions are assigned to solve for the resulting heat flux. Figure 3 shows Two-dimensional mesh free stress analysis from micrographs. OOF2 was used to calculate the overall thermal conductivity of the composite at 50°C. For doing this, a constant temperature boundary

condition of 100°C and 0°C was assigned to the bottom and top boundaries of the finite element mesh respectively so that the average temperature was 50°C. The left and right side boundaries were made adiabatic so as to make the heat transfer one-directional similar to that in flash diffusivity technique. The conventional heat flux equation was solved by the conjugate gradient method using a linear driver.

The effective conductivity of the microstructure was calculated based on the integrated heat flux value at the top boundary using steady state heat equation (Bakshi, Patel, & Agarwal, 2010).
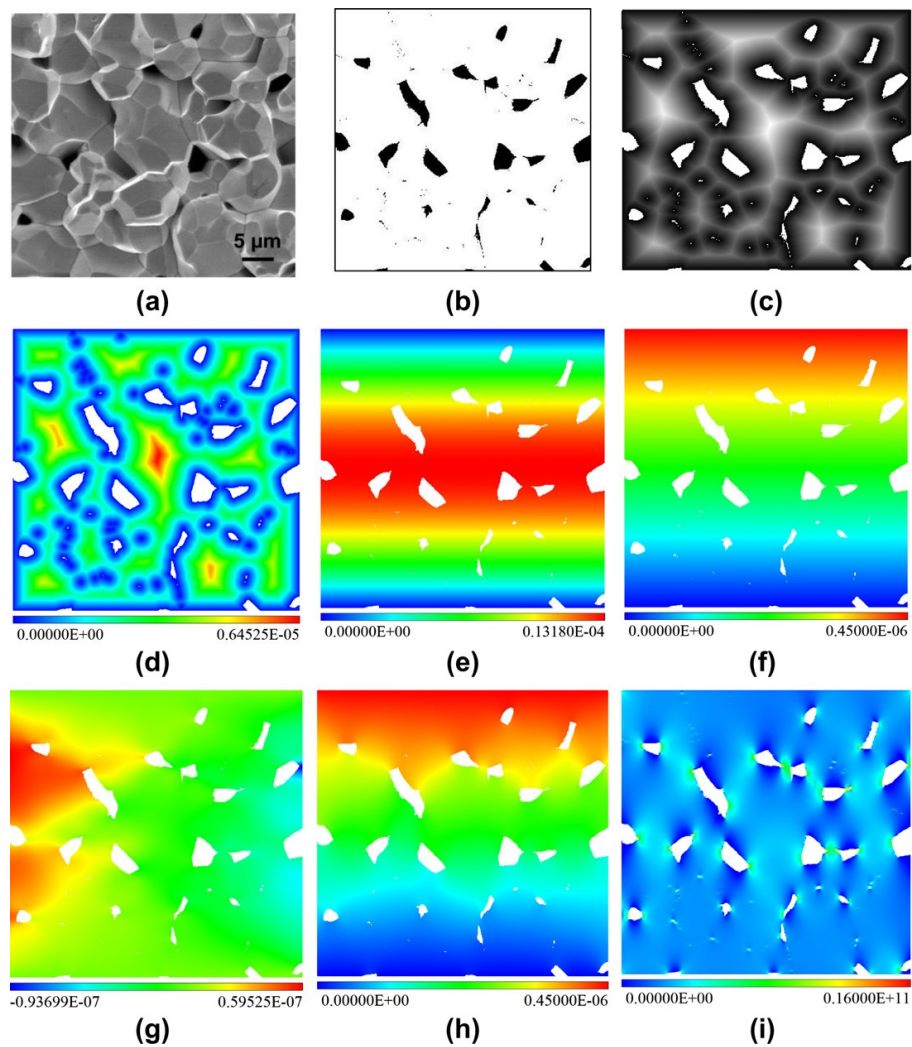

Figure 3. Two-dimensional mesh free stress analysis from micrographs.

(a) SEM micrograph of fracture surface of TaC-2200 sample. An image segmentation result in a binary image (b) where white color depicts material and black color corresponds to the pores. (c) Two-dimensional distance transformation results in an image, where intensity of the gray color depicts the distance to the nearest boundary pixel. (d) Least square fitting of B-splines to the gray values in (c) results in a smooth distance field. (e) Portions of the zero set of the distance field in (d) are used to specify boundary conditions for the analysis. Analysis results: (g, h) horizontal and vertical components of the displacement vector; (i) σy stress in porous ceramic material (shown on the scale from 0 to 16 GPa) (Bakshi et al., 2011).

OOF has advantage is to combine data in the real form of microstructures such as particle size, shape, spatial position and real orientation with fundamental material parameters including elastic modulus, Poisson's ratio, coefficient of thermal expansion (CTE) of the constitutive phases to understand the overall material behavior. This analysis technique has been employed extensively to numerically simulate mechanical and thermo-physical properties of coatings and composite materials in recent years (Azarmi et al., 2009). The analysis by OOF confirmed the findings of the statistical model, methods indicate that cracks and pores in contact affect the heat conductivity more than crack angle, free cracks and free pores. The statistical model is based on ten observations only and should thus be considered tentative, but it does allow the relationship between the porosity and heat conductivity to be suggested, and this suggestion is confirmed by OOF (Tano, 2012).

Why OOF2?

- Can use TEM, SEM and Commercial FEM packages, however it best suited to domains with clean mathematical descriptions.
- It affects the microstructure aggregate properties

- It deals with irregular structure which is important

- It's possible but tedious to construct a microstructural FEM mesh in a commercial code

OOF2 offers:

- Rapid construction of meshes adapted to irregular microstructural geometries

- Constitutive rules expressed in materials science terms

- User extensibility of constitutive rules

- Convenient parametric variations

- Virtual experiment

CHAPTER 3

Sample Preparation and Experiments

This chapter describes the experimental procedure used throughout the course of research. These include selection of materials, binders, process involved, production method, characterization and facilities and lessons learned.

3.1 Methodology and Lab Equipment overview

As an overview the copper powder was fully mixed with the spacer material with various compositions and then compaction with space holder material. The process consisted of three main steps, which involved the mixing of starting materials, compacting and heat treatments as shown in Figure 4.
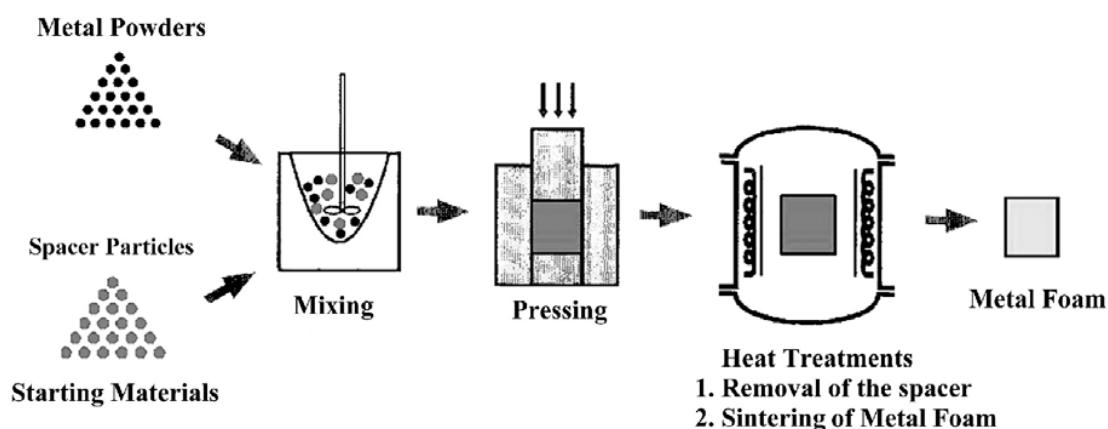
Figure 4. The graphic processing steps of the powder metallurgical process used to make the foam. (C.E. Wen, 2001)

First the copper powder and the space holding material were completely mixed together, then it was compacted into cylindrical specimen under pressure of 375MPa and heat treated in a vacuum furnace. The heat treatments were carried out in two steps. The first step was performed at 200°C holding for 30 min to evaporate the PVA; and the second step was carried

out at 850°C when the spacer was Sodium carbonate and sodium chloride. 970°C holding for 4 hours for potassium carbonate for sinter the copper powder into a porous structure. Porous copper specimen with micro-porous and macro-porous structures was found after heat treatments. Scanning electron microscope (SEM), computed tomography (CT) and Object-oriented finite element (OOF) were used to observe and analyze the image obtained from SEM. More details are found in the following sections.

3.2 Materials Selection.

The starting material was commercially pure copper powder SM400105R with 99.7% purity and 40μm size supplied by Art Molds. The selection of spacer material was based on the structure and applications of space holder as a good candidate as a spacer and ease of complete removal. The effort in this research was to create process that is environmentally friendly and economically feasible. Sodium chloride, sodium carbonate and potassium carbonate are inexpensive and readily available. Environmentally, it is friendly and can easily be burnt out when the temperature is raised or removed via dissolution as evident from study of TGA data in the literature.

The weight amounts of the metal powder to the amount of space holder were calculated to obtain various porosities in the open cell type sintered compacts. The material removal rate was calculated based on the weights before and after sintering equation. The larger particle size for the space holder and fine particle size for copper due to both larger copper particles distribution with a high average size of space-holder 200-500μm; on the other hand, the choice of a copper powder of irregular shape and small average size would improve the sintering of the compact and helping to offset the loss of mechanical strength inherent in the porosity.

Table 1

The properties of copper, Sodium chloride, Sodium carbonate and Potassium carbonate

Properties	Powder characteristic	Space holder		
	Copper	Sodium Chloride	Sodium carbonate	Potassium Carbonate
Chemical	Cu	NaCl	Na_2CO_3	K_2CO_3
Density	8.96 g/cm³	2.16 g/cm³	2.54 g/cm³	2.29 g/cm³
Melting point	1085 ∘C	801°C	851°C	891°C
Particle Size	40 μm	250-300 μm	200-400 μm	250-500 μm

3.3 Ball Mill

Using a lab high-energy vibratory ball mill variable speedball mixer, CIT-VBM-V80, was used to mix powders. It has a HP motor with a speed 1200 RPM, 200 Watts and the capacity is 50/80 ml as shown in Figure 5.

3.4 Binder

Choosing suitable binders depends on certain criteria. The literature on porous cooper was used ethanol. Poly vinyl alcohol (PVA) was used in this study, its binding ability and its rheological properties. The binder forces glue the metal particles onto the core and interconnect the particles. It is generally agent kept at a minimum in the suspension. In this study 1.5g of PVA Mw89000, 99+% hydrolyzed was add to 14.5g of water at 70°C to create a binder.

Figure 5. High-energy vibratory Ball Mill.

PVA solution was added to the metal powder prior to compaction. This helps homogenous attachment of powders on spacer. In general, the amount of binder added to powder mixture depends primarily on the relative amount of space holder. As the volume percent of spacer powder in mixture increases, the quantity of binder needed to cover all the powder.

3.5 Mixing Process

At the beginning, the copper powder was fully mixed with the spacer material with various compositions using Pyrex for 5 minutes as shown in Figure 6. For producing each powder compact of copper powder with of space holder were selected in order to obtain the predetermined porosities. Firstly the copper powder and the space holding material were thoroughly blended together. Thereafter, the PVA solution was added to cover the powders prior to compaction.
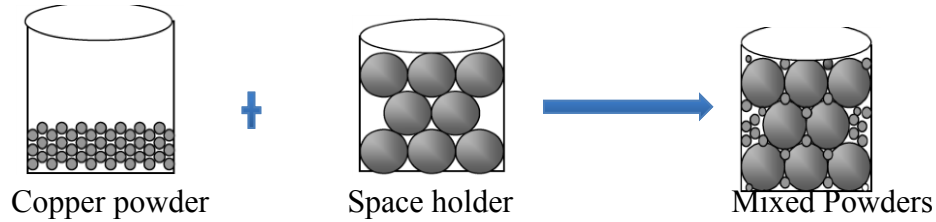
Figure 6. Copper powders mixed with the spacer material.

The mass of the metal was calculated by using equations 1 and 2 and the amount of the binder added to powder mixture was about 5 % of the total amount as previously mentioned in based on amount of spacer material.

$$M_A = \frac{M_T}{\frac{\rho_B}{\rho_A}(\frac{1}{\vartheta_A} - 1) + 1} \qquad (2)$$

$$M_A + M_B = M_T \qquad (3)$$

$M_A = Mass\ of\ metal\ in\ grams$
$M_B = Mass\ of\ space\ holder\ in\ grams$
$M_T = Total\ mass\ of\ the\ metal\ and\ the\ space\ holder\ in\ grams$
$\rho_A = Density\ of\ the\ metal\ in\ g\ /\ cm^3$
$\rho_B = Density\ of\ the\ space\ holder\ in\ g\ /\ cm^3$
$\vartheta_A = Volume\ fraction\ of\ the\ metal$

3.6 Powder Compaction

After the ingredients were thoroughly blended, 25 grams of powder using 25mm diameter die set. The mixture was uniaxial pressed using a hydraulic press into cylindrical compacts. The Carver hydraulic press is Model 3856, a twenty-two ton, manual, four-column hydraulic lab press with digital heated platens. Easy-to-read dual scale analog gauge, reading in pounds force and metric tons as shown in Figure 7.

Figure 7. The lab hydraulic press with digital heated platens.

The pressure applied on the compacts was 375MPa and was held for 90 seconds, this pressure was enough to hold the powder together. In addition, the compaction pressure for the metal powder and space holder mix must be high enough to give green strength so that it will retain its geometry throughout the sintering process.

3.7 Dissolving Process

The next step in the process was the dissolution of the space holders, using a hotplate stirrer with a magnet, the unit can boil 400 mL of water in approximately 25 minutes as shown in Figure 8, made by Carolina world class support for science and math. The sample was immersed in a 70°C hot water for 15 minute to 3 hours. The spacer dissolution took place in two steps. The first step, in case of sodium chloride and sodium carbonate, before heat treatment (sintering stage) the specimen was placed on hotplate in a beaker full of water with a magnetic bead stirrer to leach out the some of space holder. The dissolution step is an important rate-limiting step; in large samples, it takes a long time to dissolve most of the spacer and then finally the samples are

dried.

Figure 8. Hotplate stirrer with magnetic field

For the samples of porous copper made using potassium carbonate as space holder, an initial dissolution proved to be inoperable because the specimen disintegrated during repeated attempts at pre-dissolution. Therefore, these sets of samples were sintered first then the dissolution step followed. Observation and measurements showed that some particles remain in the porous structure leading to a higher relative density, and potential corrosion problems.

3.8 Heat Treatment and Sintering

A further important stage in the production of porous metal is the heat treatment. Heat treatment was carried out in two phases; during the first stage the spacer core and the binding agents are removed, in the second phase the aggregation of the metal powders to a solid metal took place.

In this process, the equipment used was furnace GSL 1700X, vertical high temperature vacuum tube shown in Figure 9. Furnace GSL-1700X is a certified high temperature vertical tube furnace using $MoSi_2$ as heating elements and 4" diameter high purity alumina tube. It is

designed for heat treatment of all types of new materials under vacuum or other gases condition up to 1700°C. High precision SCR powder controller with accuracy +/-1C and 30 segments programmable up to 1700 ^{o}C control the temperature of GSL-1700X of furnace.

As known the density of argon is heavier than air and because of that a fill and purge process was used after sealing the samples in the tube. The sealed tube was initially vacuumed and then the tube was refilled with argon and then again the tube was vacuumed. The maximum vacuum level provided by the pump was -27 Psi.

The gas flow systems specific are as follows:

- Vacuum furnace to -27 Psi,

- Fill the chamber with argon to 0 Psi

- Evacuate the furnace chamber Vacuum to -27 Psi

In this study, the samples were heat-treated using the vacuum furnace to remove the space holder material followed by high vacuum furnace to sinter the powder compact to get the porous structure. A vacuum is necessary because of copper's affinity towards oxygen and its tendency to form copper oxide in the presence of heat and oxygen.

Figure 9. Furnace GSL - 1700X.

The heat treatment was conducted in two steps; one in order to remove the space holder and then next to sinter the parts. The samples were heated at 200°C for 30 minutes and then raised heated again to 850°C or 970°C °C holding for 4 hours according to the sample then cooling to the room temperature.

3.9 Characterizations of Samples

3.9.1 Density measurement. The density determination was performed by means of Archimedes' principle, which states that a body immersed in a fluid apparently loses weight by an amount equal to the weight of the fluid it displaces. This method allows determination of the density of solids, viscous and pasty substances, as well as liquids.

Figure 10. Mettler Toledo's density kits

In order to determine the density of a solid porous substances the Mettler Toledo's density kits is precise for both analytical and precision balances. The kits are easily mounted on balance in a few simple steps.

3.9.2 Scanning electron microscopy (SEM). After samples are mixed, pressed sintered and the space holder was removed the scanning electron microscopy (SEM, HITACHI-SU8000) shown In Figure 11, with an operating voltage of $10 \sim 20$ kV, 2A current was used to carry out a more detailed characterization of the morphology. SEM has excellent features like ultra high-resolution imaging technology, wide ranges of signal detecting system, and user-friendly operation.

Figure 11. HITACHI-SU8000 Scanning Electron Microscopy

3.9.3 Computed tomography (CT). In addition to the SEM in order to acquire images for use in modeling the Phoenix Nanotom M is the nano CT system that was used. CT is quite useful for scientific and industrial computed tomography 3D metrology on a wide sample range. The GE Phoenix nanotom- M 180, GE sensing & Inspection Technologies GmbH, Germany) shown in Figure 12, X-ray parameters used were 80kV, 180μA and number of projections (N_p) was 1,800. Reconstructed data were investigated through VG Studio Max 2.1 software. Figure 12 shows the CT scan machine.

Figure 12. Computed tomography CT

The system realizes a unique spatial and contrast resolution on a wide sample and application range especially with metal analysis. Fully automated execution of CT scan, reconstruction and analysis process ensures its ease of use as well as fast and reliable CT results. Once scanned, the fully three dimensional CT information allows many possibilities for analysis.

3.9.4 Compression test. The last physical test conducted on the prepared samples was compression. The ASTM standard E20 was referenced to ensure standards. The MTS Model 810 Material Testing System was used to determine the compressive strength. A custom

fabricated pressure tension device designed to test 25 mm diameter by 12 mm long specimens was used to perform the pressure strength tests. MTS 810 Testing System was hosted by Center for Composite Materials Research (CCMR) that can be configured to meet different testing needs. The machine is model #318.25, its force capacity is 250 KN (55 kips), and it measures axial force over a displacement range of +/- 2.5 inches as shown in Figure 13.
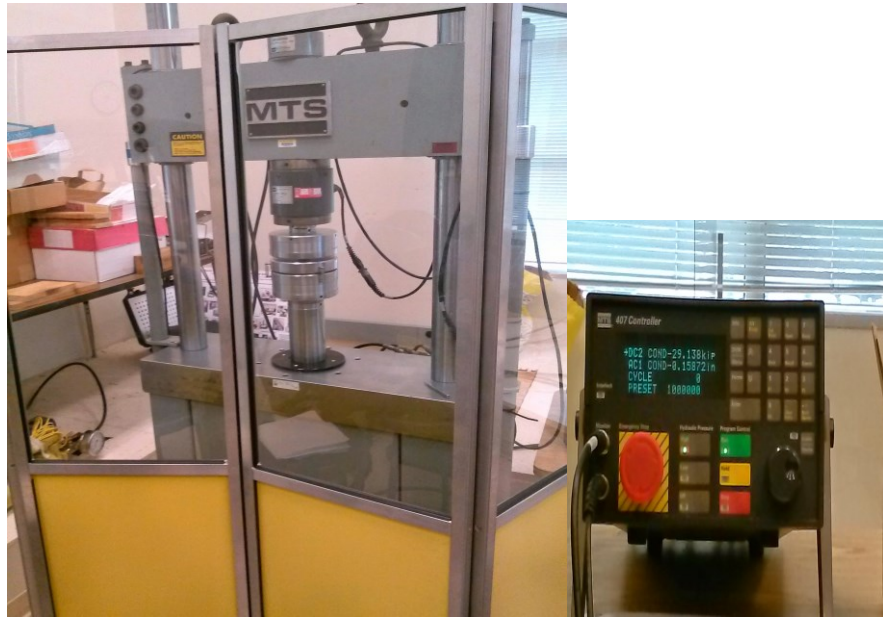
Figure 13. MTS 810 compression test with 407 digital controller.

The system software was running on a personal computer and working with the 407 digital controller these functions provide a full range of loading functions and data capture options.

3.9.5 Object oriented finite element. Object-oriented finite element (OOF) developed by the National Institute of Standards and Technology (NIST), USA. OOF 2.1.9 package, installed in a Linux Mint 16 Cinnamon 32-bit system, comprises a preprocessor interface to correlate the real morphological images to the micro/nanostructures, generate the mesh grids with assigned material properties and apply the loading and boundary conditions to the domain, as well as the solver with a postprocessor OOF for the contour illustration of stress/strain state in

each element. Object-oriented finite element software (OOF) main page shown in Figure 14. The finite element analysis was conducted on a Hp Compaq 6720s using 2 GHz processors and 2 GB RAM.
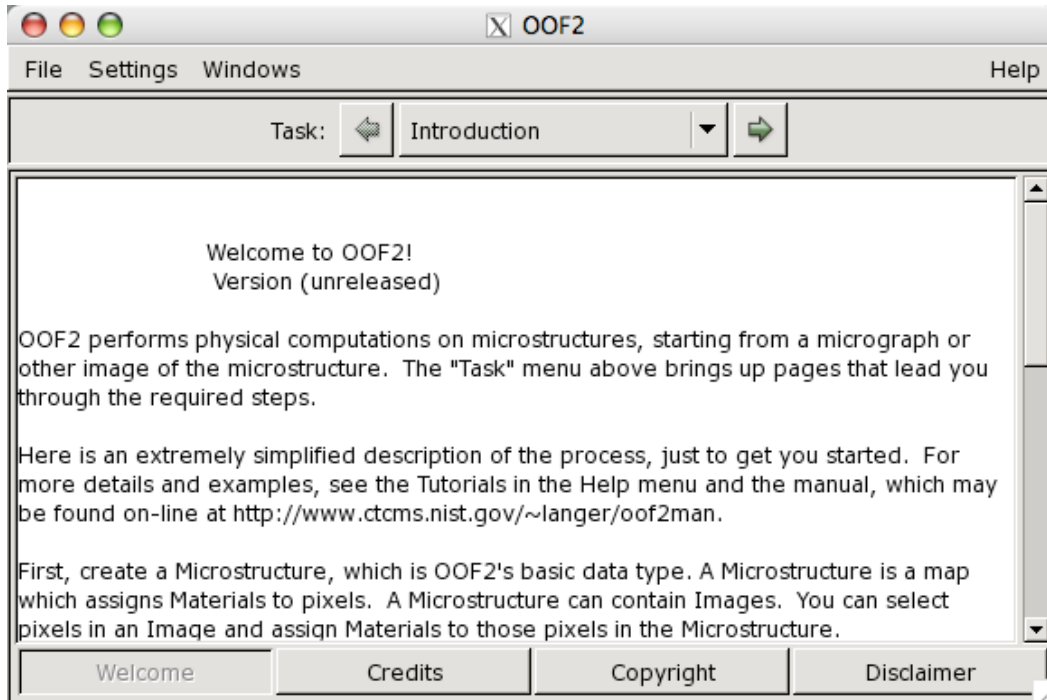

Figure 14. Object-oriented finite element (OOF) main page

Firstly, a characteristic region of interest in Figure 17 was selected from a typical SEM micrograph of titanium foam. Then the image segmentation using the pixel selection tool was employed to assign the material properties. The 2-D finite element mesh was then created based on OOF skeleton to display all the details of micro/nanostructures titanium foam with the actual size and shape, orientation and spatial position. The mesh generation began with the conformity of right triangular or quadrilateral elements over the foam and then was followed by the mesh refinement process using an energy functional minimization approach. This outline does not increase the total number of elements due to the element sectors arising mainly in the interfaces, thus reducing computational time during the simulation.

CHAPTER 4

Results and Discussion

As part of the purpose of the research was to investigate the porosities, compressive strengths of porous copper using three different space holders made through dissolution sintering technique. This chapter presents and discusses the procedures, the characterization and OOF modeling results of the samples made through scan electron microscopy SEM, computed tomography CT.

4.1 Powder Compaction

In this study, the powder mixtures with spacers were compressed using the hydraulic press with a pressure of 375MPa and held for 90 seconds. The variation in densities and dimensional controls were the problems encountered in the compacting the materials. An optimization study was pursued in this research after which the two binders were investigated, these include: ethanol and PVA, PVA was selected because of its ability to hold the green form together and not causing an adverse effect on the chemical reaction with the mixtures.

4.2 Sintering Cycle

An optimal sintering condition was selected in order to attain good mechanical properties as well as dimensional control of the sample. The process cycle for all samples involving sodium chloride (NaCl) as space holder is shown

Dissolving   ⟶   Sintering   ⟶   Dissolving
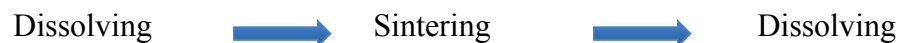
The samples were immersed in a hot water at 70°C for 2 hours and then heated in the furnace at the rate of 10°C/min up to 200°C in order to evaporate the water and PVA completely followed by heating it at 5°C/min up to 850°C and held at this temperature for 4 hours and later

cooled to room temperature at the rate of 10°C/min. It was then placed under running water for 20 minutes. Figure 15 shows the heating process for all space holders; porous copper using sodium chloride, sodium carbonate and potassium carbonate.
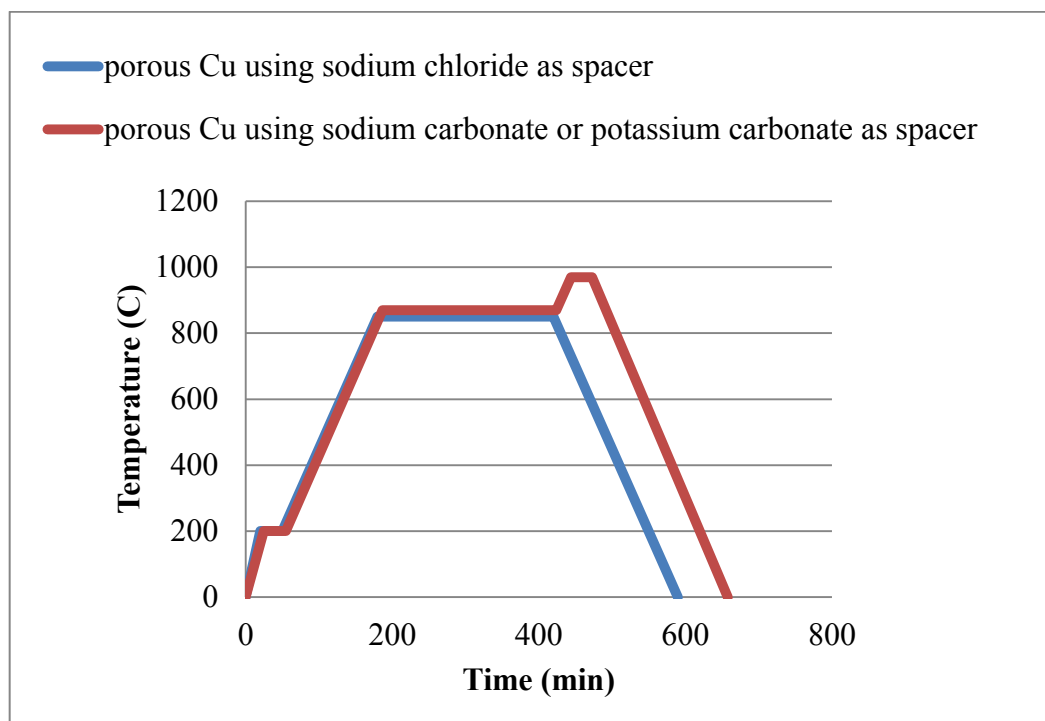
Figure 15. The heat process porous copper using sodium chloride, sodium carbonate and potassium carbonate as spacer

For the samples with sodium chloride and sodium carbonate as spacers, the process involved suspending the samples placed in tea sieve in water at 70°C and magnetically stirred for 30 minutes and then placed the samples in a furnace of a vacuum environment at 10°C/min up to 200°C to evaporate the water and PVA completely. Then the process continued by heating it to temperature up to 870°C at rate of 5°C/minutes and held it for 4 hours then reheated up to 970°C using 5°C/min and finally cooled to room temperature. When the heating process has completed, the sample was placed below running water for 15 minutes.

4.3 Effect of Sintering

     4.3.1 Using NaCl as space holder. The sintering and dissolution process was successful for the porous samples. This work infers that a weight measured of the samples in the green stage and a weight measured after the spacer has been removed displayed a percentage reduction which equals the partial amount of initial weight of spacer material added to the mixture. Table 2 shows the actual effect of sintering in the form of total weight reduction of sample before and after sintering the samples.

Table 2

Weight reduction before dissolving, sintering and after dissolving for Copper material and NaCl spacer

Sample (Volume ratios)	Weight of space holder (g)	Weight pre-dissolving (g)	Weight post Sintering (g)	Weight after dissolving (g)	Total Weight reduction %
Cu +NaCl (1:1)	4.86	24.85	22.27	21.21	14.65%
Cu +NaCl (1:2)	8.70	24.51	19.06	16.49	32.72%
Cu +NaCl (1:3)	10.50	24.68	18.30	14.38	41.73%
Cu +NaCl (1:4)	12.27	22.31	13.75	12.36	44.60%

     From the Table 2 it is clear that the space holder was only partially removed.   It is also shown that the difference in weight increases as the volume fraction of spacer material increases, for example reduction is found to be 14.65% in the range of 0.5 volume fraction of copper and

44.60% for the volume fraction of 0.2 of copper to NaCl. Figure 16 graphically displayed the weight reduction after dissolution.
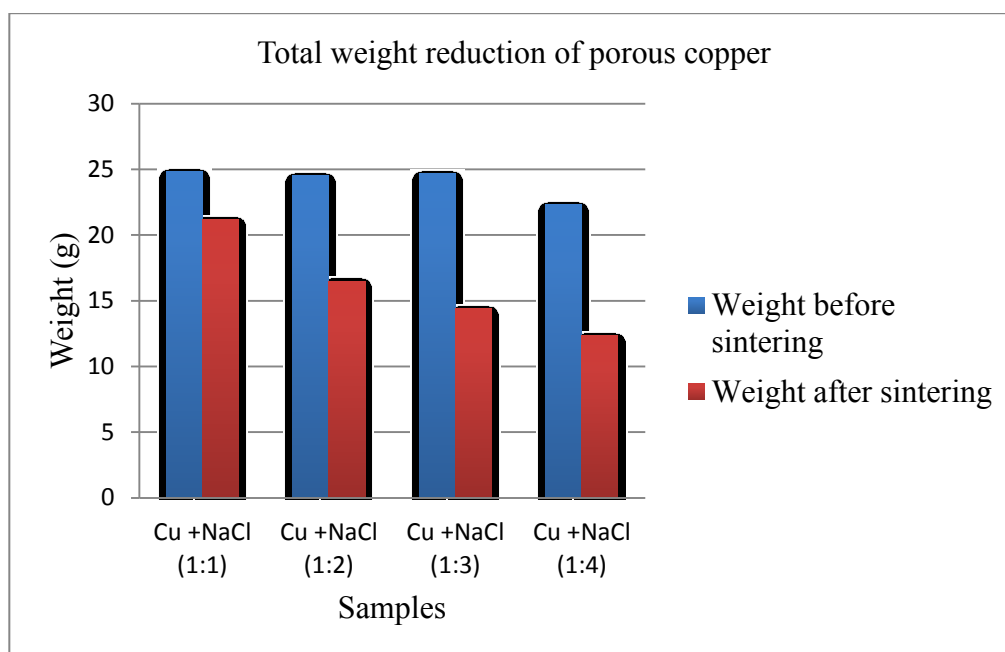

Figure 16. Total weight reduction after sintering process using NaCl as spacer

4.3.2 Using Na₂CO₃ and K₂CO₃ as space holders. The result of reduction in the weight for porous copper using **Na₂CO₃** as space holder is found to be in the range of 8 to 19.5% for all the samples as shown in Table 3. This outcome indicates that the space holder was partially removed. The result of reduction in the weight for porous copper using K_2CO_3 as space holder is found to be in the range of 2 to 7% for all the samples as shown in Table 4. The low % reduction means that lower amount of spacer was remaining and more study is needed to be done to optimize the process for K_2CO_3 removal. Additionally the visual studies and SEM works are displayed in the section 4.5 which verified residual K_2CO_3 in the samples.

Table 3

Weight reduction after sintering process using Na₂CO₃as spacer

Sample (Volume ratios)	Weight of space holder (g)	Weight pre-Sintering (g)	Weight post Sintering (g)	Weight after dissolving (g)	Total Weight reduction %
Cu +Na$_2$CO$_3$ 1:1	5.52	25.00	24.76	22.78	8.88%
Cu +Na$_2$CO$_3$ 1:3	8.73	17.97	17.47	14.06	19.48%

Table 4

Weight reduction after sintering process using K₂CO₃ as spacer

Sample (Volume ratios)	Weight of space holder (g)	Weight pre-Sintering (g)	Weight post Sintering (g)	Weight after dissolving (g)	Total Weight reduction %
Cu +K$_2$CO$_3$ (1:1)	6.11	28.75	28.61	28.24	2.02
Cu + K$_2$CO$_3$ (1:3)	8.68	19.27	18.74	17.92	7.00

4.4 Principle of the Density and Porosity Determination

The density and porosity of the consolidated samples were measured using Archimedes principle and ethanol was used as auxiliary liquid. Equation (1) & (2) show the equations used for determination of density and porosity. The density of a solid was determined with the aid of a liquid whose density ρ_0 is known (ethanol are usually used as auxiliary liquids). The solid was weighed in air (A) and then in the auxiliary liquid (B). The density ρ was calculated from the two weighing equation as follows:

$$\rho = \frac{A}{A-B}(\rho 0 - \rho l) + \rho l \,............(4)$$

ρ = Density of sample

A = Weight of sample in air

B = Weight of sample in the auxiliary liquid

ρ_0 = Density of the auxiliary liquid

ρ_l = Air density (0.0012 g/cm³)

Density values of C2H5OH taken from "American Institute of Physics Handbook" at 22.6°C is 0.78712 g/cm³

$$Porosity = \frac{Theoretical\ density\ of\ copper - density\ of\ sample}{Theoretical\ density\ of\ copper} \,.......(5)$$

The theoretical density of copper 8.96 g/cm³

Relative density equation

$$Relative\ Density = \frac{Density\ of\ sample}{Theoretical\ density\ of\ copper} \,.............(6)$$

Table 5

Density, relative density and porosities of porous copper

Samples(…)	Density g/cm³	Relative density %	Porosity %
Cu +NaCl (1:1)	5.177	57.78	42.22
Cu +NaCl (1:2)	4.940	55.13	44.87
Cu +NaCl (1:3)	4.864	54.28	45.71
Cu +NaCl (1:4)	3.782	42.21	57.79
Cu + Na_2CO_3 (1:1)	4.010	44.75	55.24
Cu + Na_2CO_3 (1:3)	3.047	34.00	65.99
Cu + K_2CO_3 (1:1)	3.938	34.95	56.05
Cu + K_2CO_3 (1:3)	3.791	42.31	57.69

Using the space holder technique porous copper with the porosities in the range of 40 – 66% were produced. The calculated values of porosities and densities are shown in Table 5 for the three space holder materials. These values are plotted for all the space holder materials with different volume fractions.

Table 5, it is obvious that decrease in the density increases with the porosity and it can be seen that the maximum porosity was achieved through space holder Na_2CO_3 of volume ratio 1 to 3 with a value of 65.99% and the lowest density is 3.047 g/cm³ using sodium carbonate as spacer and the lowest porosity is 42.22% with the highest relative density of 57.78% was obtained with 0.5-volume fraction of spacer material. The important factor is that the porosity increases with the volume percentage of spacer material added. From Table 5, porosities of sample produced using NaCl and Na_2CO_3 spacer material were lower when compared to the

samples produced using K_2CO_3.

By using 0.5- volume fraction of copper, the maximum porosity obtained among NaCl, Na_2CO_3 and K_2CO_3 space holder was 66% and 55.24% porosity was achieved by using Na_2CO_3 as spacer. But when K_2CO_3 has been used the porosity was 56.05%, which is the maximum porosity among the others.

4.5 Compression Tests

Compression testing was performed on all porous samples to determine the compression strength of the samples. Load and displacement data were obtained and was used to plot to stress stain curve. Also, pictures were taken using a digital camera. This test is a method used for evaluating compressive properties of porous copper metals. The compressive test was carried out using the test machine described in section 3.9.4 at room temperature with strain rate of 0.2 in/min. The initial height and diameter of the samples were measured to compute the calculation.

The three regions to be expected in a compression test are: a linear elastic deformation stage, a plastic deformation and pore collapse stage, and finally a densification stage as shown in Figure 17 (Cady, Gray, Liu, Lovato, & Mukai, 2009). At small strain rates the pore failure stage consists of an initial load drop due to local buckling and failure of the wall structure on a plane normal to the loading direction at the weakest region of the sample. Stresses in the failure plane will rise as the cell walls interact until the load level reaches a maximum value where the next plane of failure will occur.   Finally, the densification stage shows a rapid rise in the load carried by the sample. All of the stress-strain curves of sintered pure copper samples and samples using space holders with different volume ratios of copper samples (Figure 18-20), showed three

distinct regions of deformation. The regions for the pure copper behave much as solid metallic as compression data predicts.
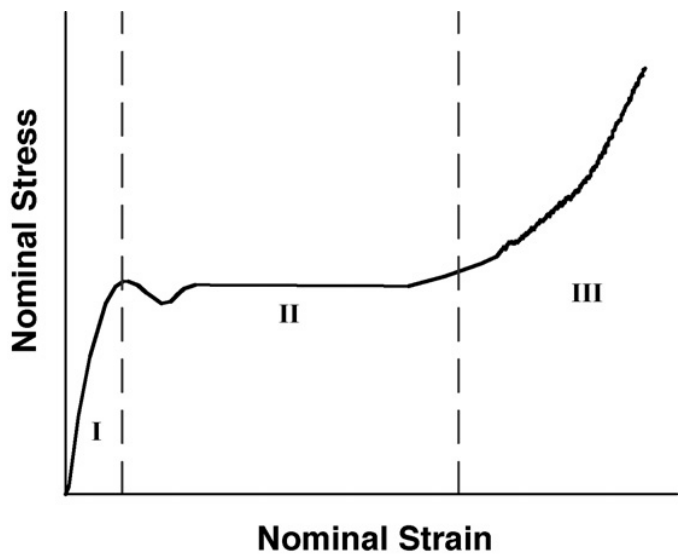

Figure 17. Model of regions of compression data for a porous sample (Cady et al., 2009)

In Figure 18 there is an elastic deformation region in which the slope is steady, a plastic region where the slope is decreasing and a large increase again when crushing occurs up to a peak stress and plastic region up to fracture. The failure may be due to the heterogeneous density and strain distributions of the porous copper specimen.
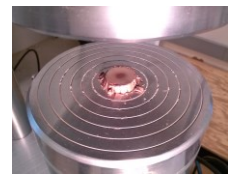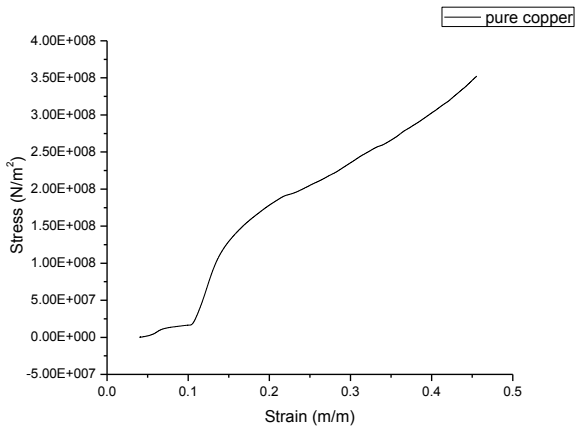
Figure 18. Stress-strain curves samples of pure copper 375 MPa.
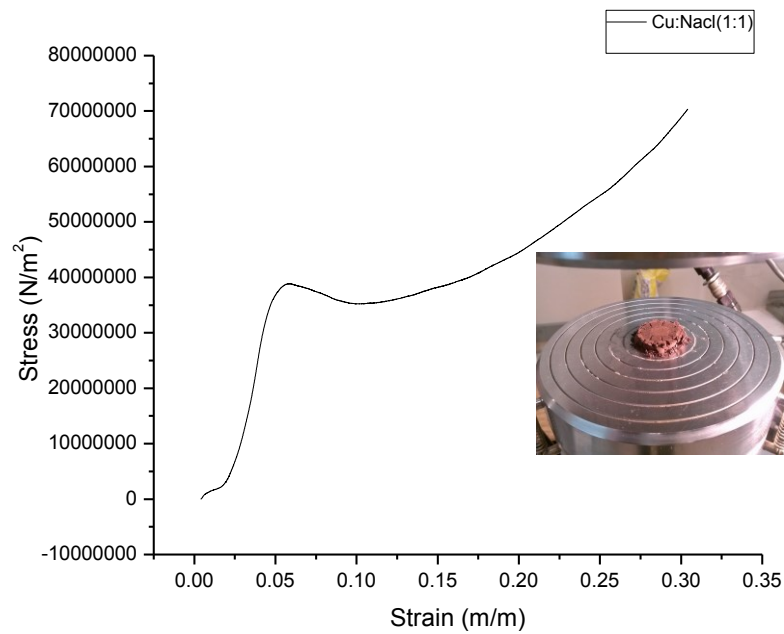
19 a)
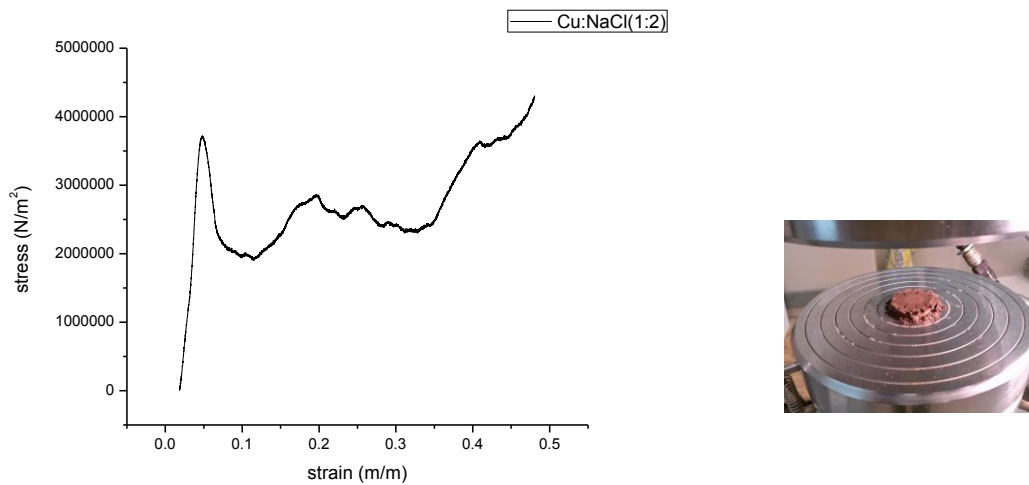
19 b)

Figure 19. a) Stress-strain curves of sintered porous copper using 0.5 -volume fraction of copper to NaCl. The insert is the samples after crushing b) Stress-strain curves of sintered porous copper using 0.33 -volume fraction of copper to NaCl.
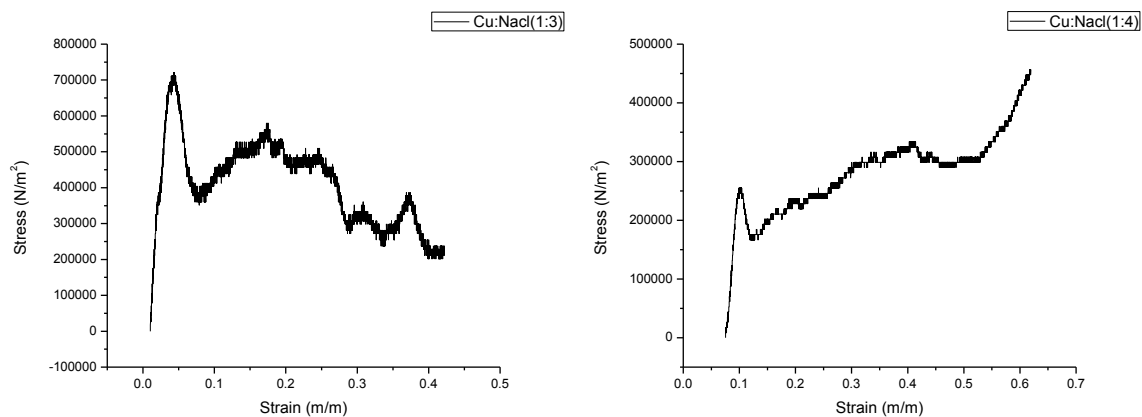
20a)   20b)

Figure 20. Stress-strain curves samples of porous copper using NaCl as space holder (a) a

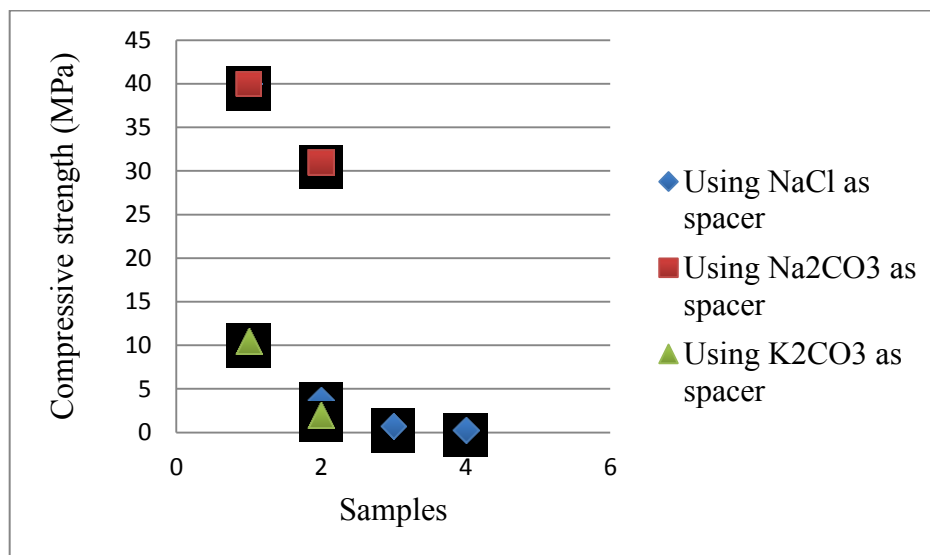sample of 0.25- volume fraction of copper to NaCl. (b) 0.2 volume fraction of copper to NaCl.

Figure 21. The compressive strength of porous copper samples using different space holders.

Table 6

Stress and strain of porous copper

Sample	Compressive Strength (MPa)	Strain (m/m)
Cu +NaCl (1:1)	40	0.065
Cu +NaCl (1:2)	3.75	0.8
Cu +NaCl (1:3)	0.75	0.075
Cu +NaCl (1:4)	0.26	0.12
Cu + Na$_2$CO$_3$ (1:1)	40	0.32
Cu + Na$_2$CO$_3$ (1:3)	31	2.7
Cu + K$_2$CO$_3$ (1:1)	10.5	0.26
Cu + K$_2$CO$_3$ (1:3)	2	1
Pure Copper	175	0.2

The relative density and the compressive strength were identified as the two main functions to evaluate porous copper quality. The relative density in porous copper metal, defined as the ratio of porous Cu density to base material density (8.96 g/cm3 for pure Cu). For example, if relative density of a porous is 0.45, then this means that metal occupies 45% of the total volume of that porous. In general porous copper using NaCl as spacer, have relative

densities ranging from as low as 0.422 up to 0.578. According to Figure 22 increasing density of porous Cu leads to an increase in the compressive strength.
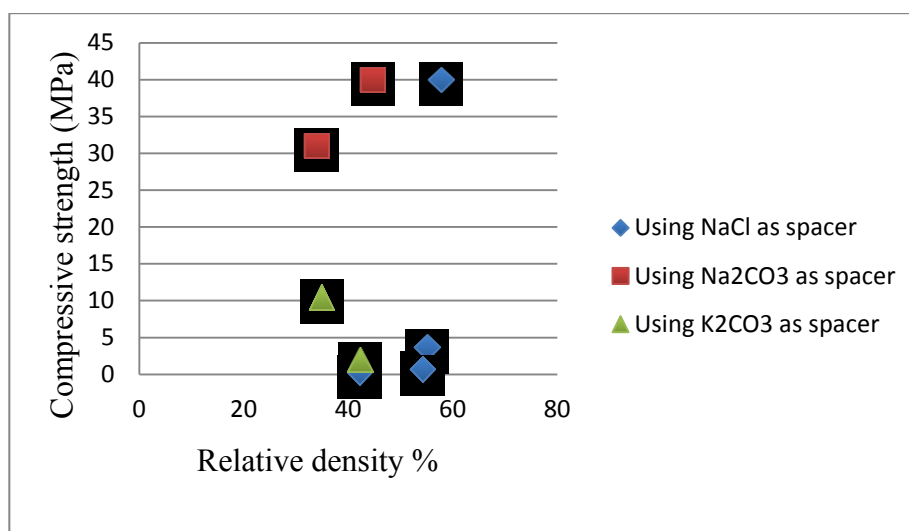

Figure 22. Shows relative density and the compressive strength

4.6 SEM Microstructural Analysis

Scanning electron microscopy (SEM) was used to study the morphology of porous copper. The morphology of samples was presented in Figure 23- 28. The secondary image capture reveals a topography characteristic of the raw powders and the open cells that were formed. The average size of the powder is around 40- 75μm according to the SEM image Figure 22 a & b. This image is the SEM micrograph indicating particles of pure copper. Notice the size bar on the bottom right of all images for size comparison. Figure 23 is the SEM image of pure NaCl in high magnification. Figure 25 shows SEM micrograph of potassium carbonate K_2CO_3 powder in low magnification

23a)   *23b)*
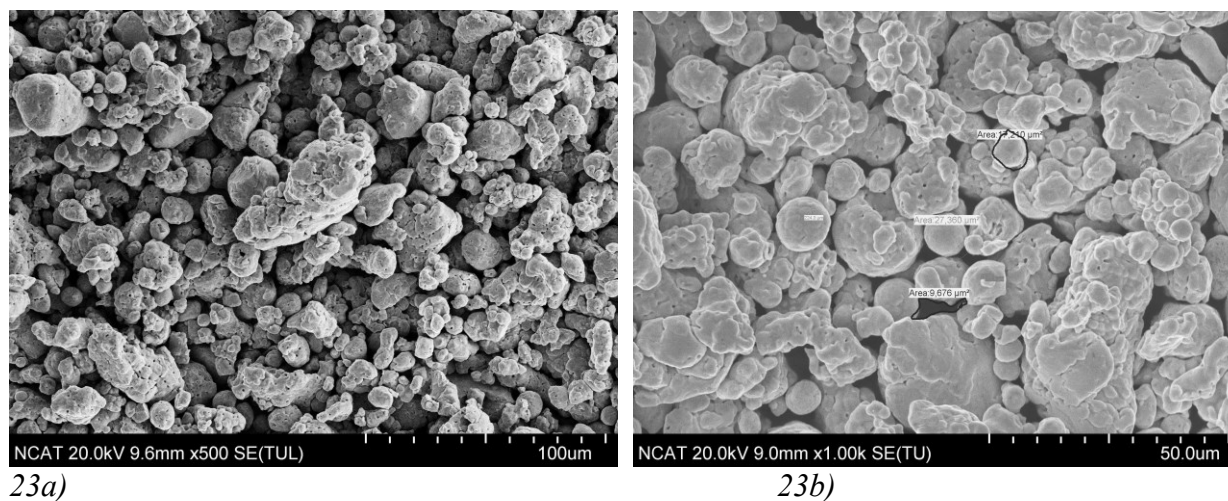
Figure 23. a&b) SEM image of copper powder in high magnification SEM image. Notice the

sintered area and a typical pore area.
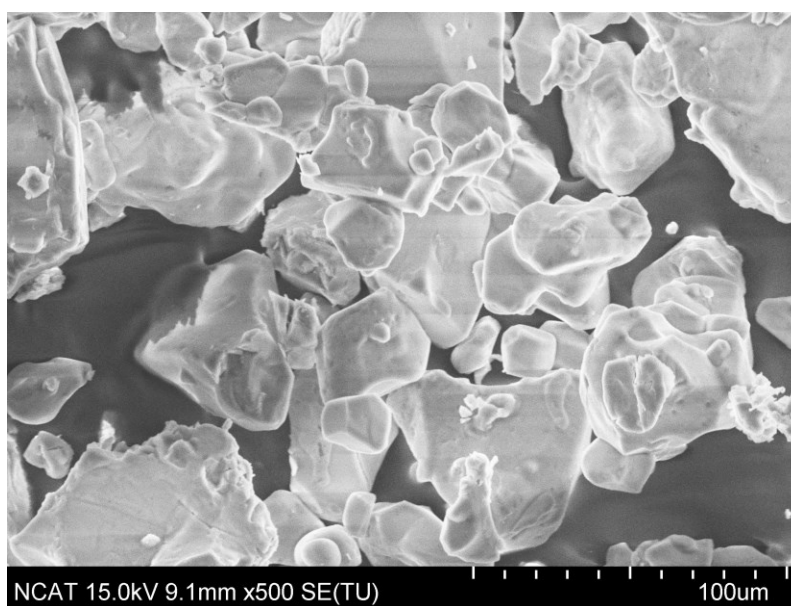
*Figure 24.* SEM image of pure sodium chloride NaCl in high magnification
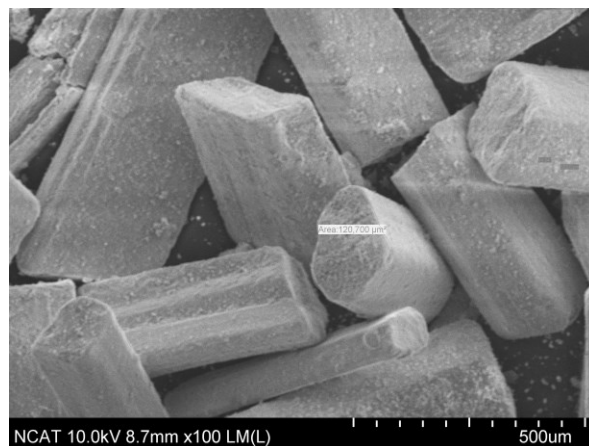
Figure 25. SEM image of potassium carbonate K_2CO_3 powder in low magnification, notice the cross section size of the powder.

The microstructure of porous copper manufactured through NaCl spacer materials with a 0.33 volume fraction of copper to NaCl after 12 hours sintering is displayed in Figures 26a and 26b. The various distributions of pores can be seen in the different micro and macro-pores sizes. The white areas seen in SEM images in Figure 26, are evidence of retained salt phase after sintering. Figure 27 shows relatively spherical pores after the removal of the space holder Na_2CO_3. Micron sized pores were also present in the matrix. It can also be observed that the pore size was smaller than that of the size of the K_2CO_3 particles; this could be due to the fact that the NaCl particles dissolved. The SEM image of porous copper using two different volume fractions of K_2CO_3 spacer material is shown in Figure 28. From the SEM image of porous copper using K_2CO_3, it is clear that the micro-pores showed a relatively uniform distribution with good closeness between space materials.
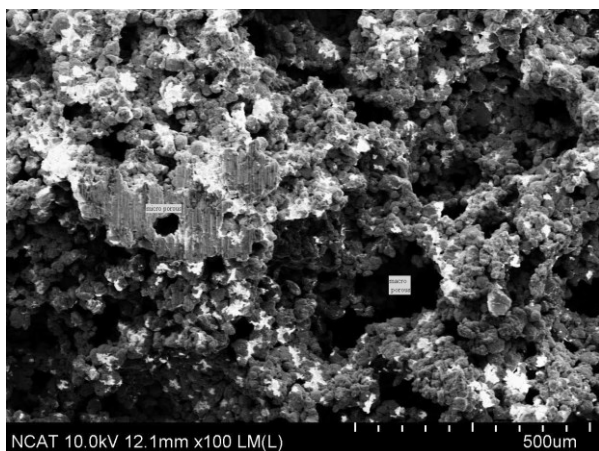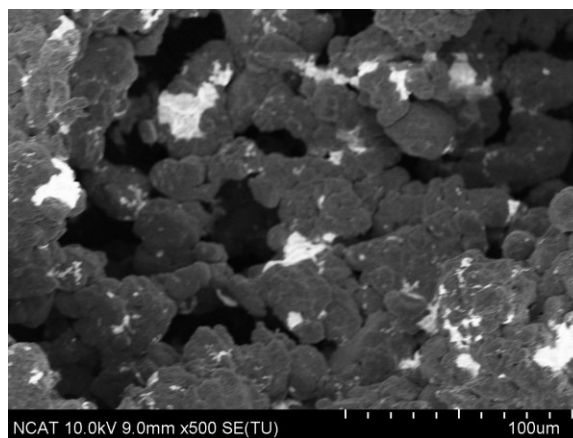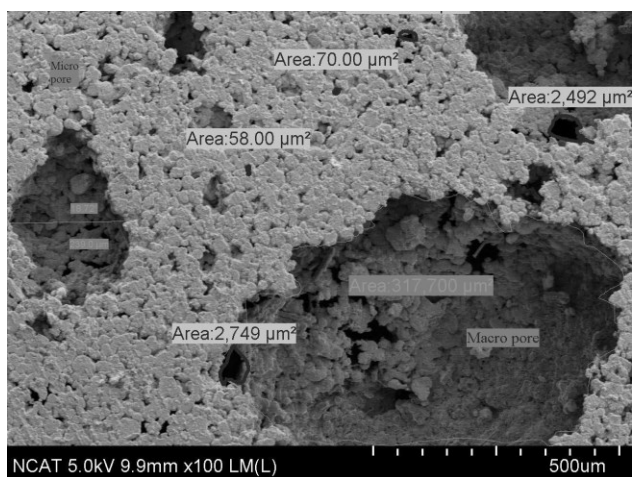
26a)   26b)

Figure 26. SEM micrograph of the porous copper fabricated using NaCl the space holder

method. 26a) Low magnification image of porous Cu using 0.33- volume fraction of Cu to NaCl.

26b) High magnification of porous Cu porous using NaCl as spacer with 0.5 -volume fraction.
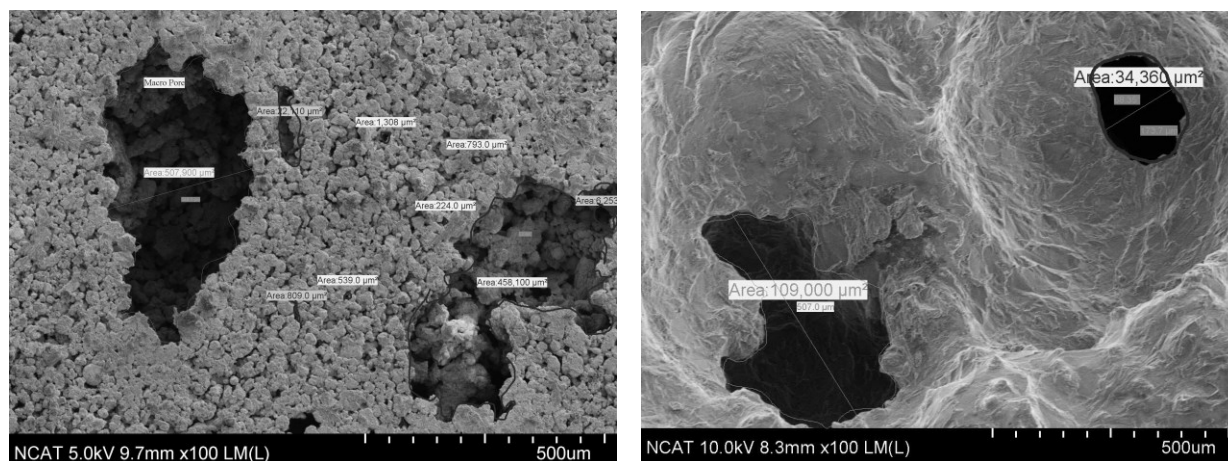

27a)   *27b)*

Figure 27. SEM micrograph of the porous copper fabricated using Na_2CO_3 as spacer. 27a) Low

magnification image of porous Cu using 0.5-volume fraction of Cu to Na_2CO_3. 27b) Low

magnification image of porous Cu using 0.25-volume fraction of Cu to Na_2CO_3

Figure 28. SEM micrograph of the porous copper fabricated using K_2CO_3 as spacer. 28a) Low magnification image of porous Cu using 0.5-volume fraction of Cu to K_2CO_3. 28 b) Low magnification image of porous Cu using 0.25-volume fraction of Cu to K_2CO_3

4.7 Nano-CT Imaging

A series of measurements of the structures of various samples of porous copper had been carried out during this study using X-ray micro-tomography (Nano-CT). As a non-destructive technique, nano-CT provides a direct way to see the images of the pores spaces as a volumetric (3D) representation of structures. A nano-CT scanner uses X-rays to penetrate from different viewpoints of a 3D object and create attenuated projection profile. For setting up the scan process in the micro CT, the items must be considered the location of sample between x-ray source and detectors to have a good magnification and resolution. The image resolution is directly related to the sample size. A smaller sample would result in better resolution at higher magnification, which means smaller voxels can be detected. The image quality was analyzed based on three parameters:

- Presence of beam hardening,
- The contrast in the image and

- The focus of the image.

Figure 29 (a) & (b) are the 2D and 3D images of experimental two-phase show the original sample in CT scan in 2D and 3D. Figures 29-30 are all resultant from the 0.25 volume fraction of copper to NaCl sample. The sample is a Figure 29b) shows the scan amended to a smaller cylindrical shape to provide a better understanding about the sample. When the ray scattering to scan process for achieving more accurate results, the model was cut down to a smaller cylindrical shape by using the virtual volume of interest in VG Studio Max.
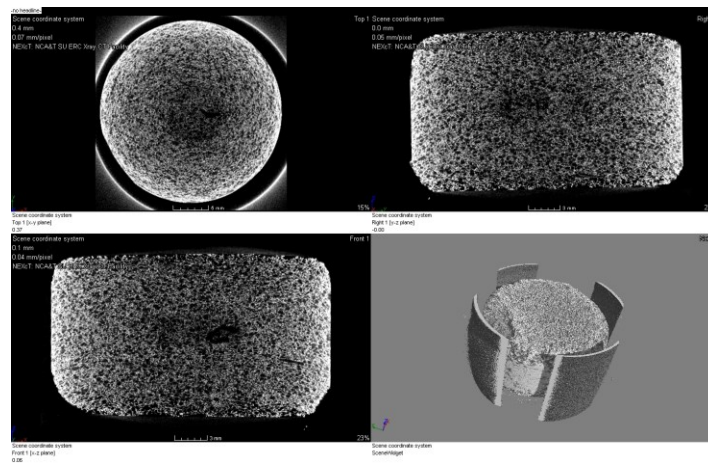

29a)
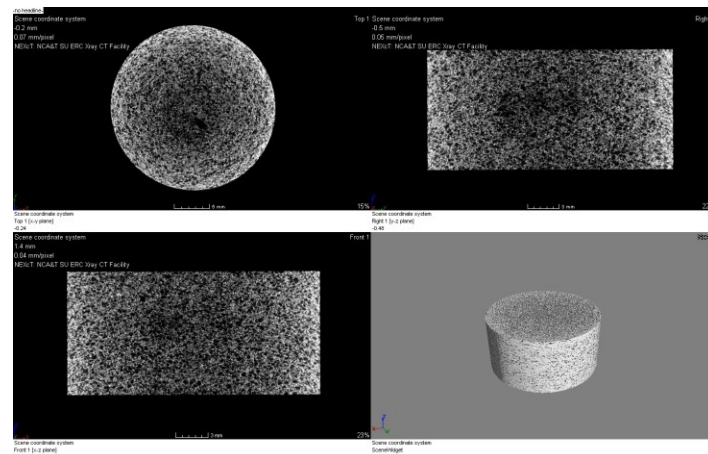
29b)

Figure 29. (a) & (b) are the 2D and 3D images created via the VGA software after the scan. a), porous copper using NaCl as space holder in CT scans. Fig 31b) shows the amended to a smaller cylindrical shape to provide a better understanding about the sample.

Figure 30 and Figure 32 show the porosity measurement technique using VG Studio Max. Figure 30 is for same 0.25 volume fraction of copper to NaCl sample as in Figure 29 whereas Figure 32 is the analysis for a 0.20 volume fraction of copper to NaCl sample. The figures display the method used to determine the porosity using VG Studio Max volume analysis. Choosing the right bandwidth between the two selected lines on the color spectrum of the model was the key to assess the porosity. Errors or misjudgment in selecting the band size can affect the measured porosity.
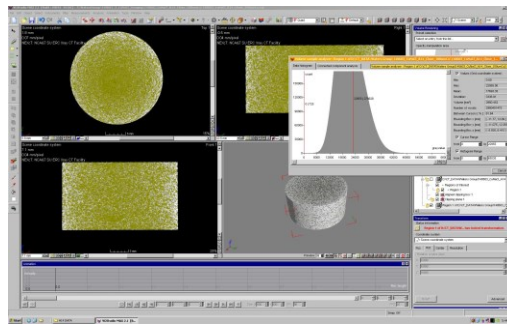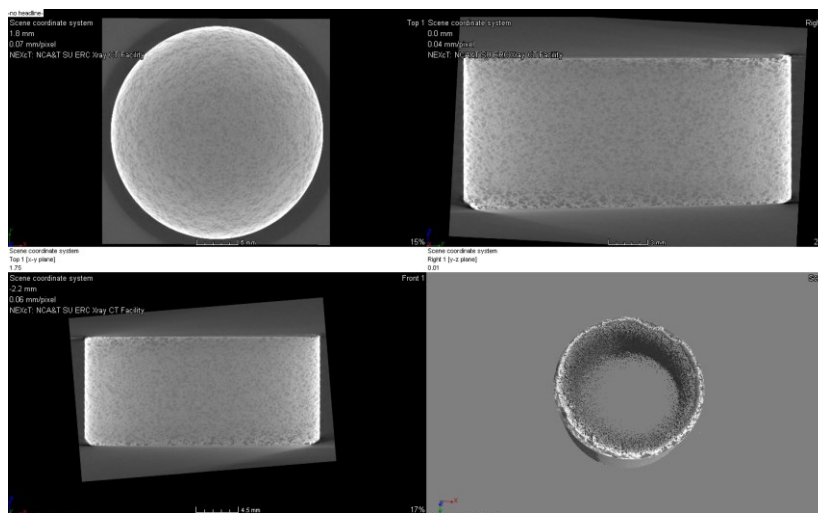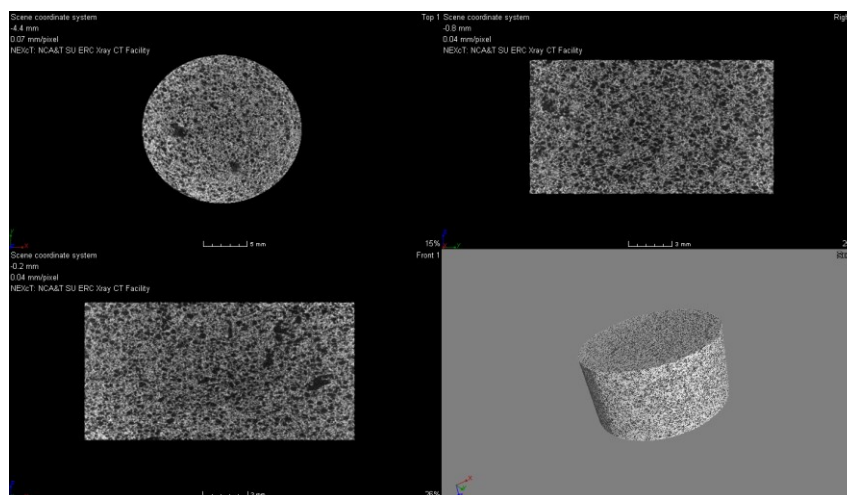

30a)
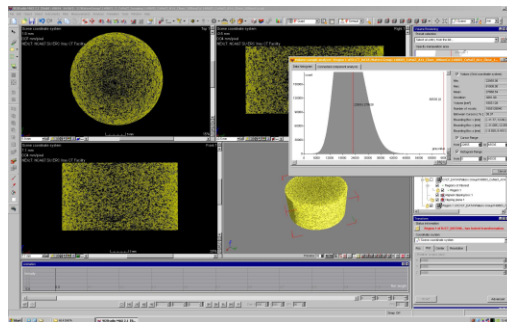
30b)

Figure 30. Shows porosity measurement techniques using VG Studio Max for open cell porous copper sample using NaCl; a.) 0.25 volume fraction of copper to NaCl b.) 0.20 volume fraction of copper to NaCl.

Figure 31a is an image of porous copper using NaCl as space holder in CT scans. In Figure 31a)

the original sample in CT scans. Fig 31b shows the modified sample shape to provide a better
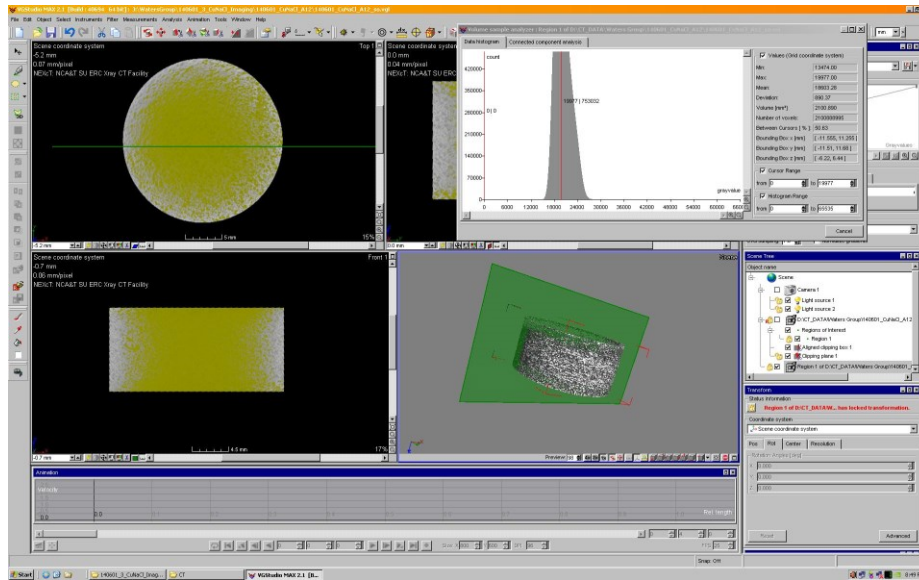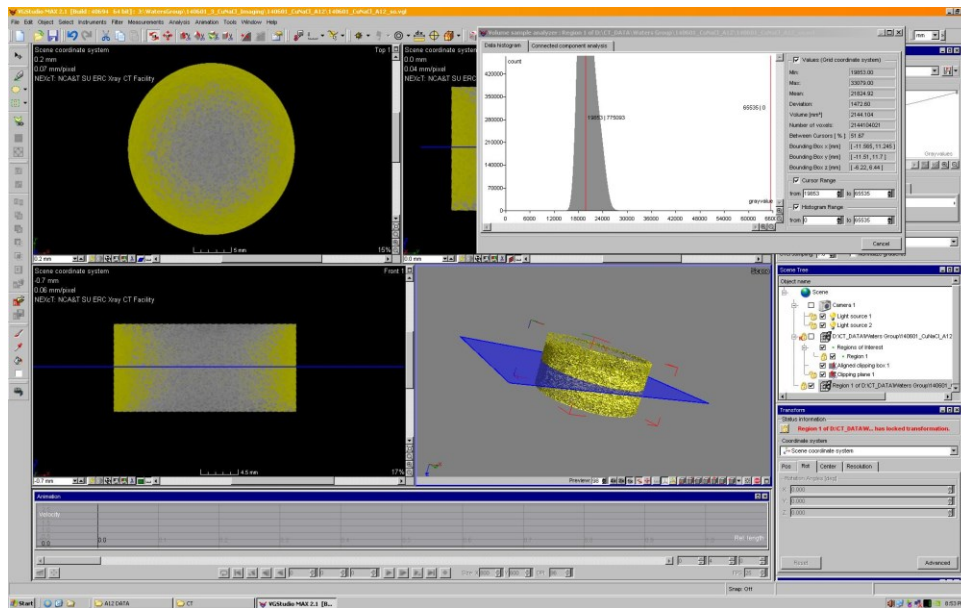
understanding.

31a)

31b)

Figure 31. (a & b) are the 2D and 3D images of open cell porous copper sample using NaCl,

volume fraction is 0.33 copper.

32a)

32b)

Figure 32. (a & b) show porosity measurement technique using VG Studio Max for open porous copper sample using NaCl, the volume fraction is 0.33 copper.

Assuming the similar porosity in the sample, the calculation results can be expanded to the whole sample porosity evaluation. One of the important considerations of the volume of interest selection is being ensured that the outer image errors are not in the volume boundary to obtain more accurate results.

For setting up the scan process in the micro CT, the items must be considered; the location of sample between x-ray source and detectors to have a good magnification and resolution. The image resolution is directly related to the sample size. A smaller sample would result in better resolution at higher magnification, which means smaller voxels can be detected. Comparison of Nano -CT results and Archimedes principles

Table 7

Comparison of Nano-CT result and Archimedes principles

| Samples	Porosity by CT%	Porosity by Archimedes principle%
Cu + NaCl 1:3	40.51	45.71
Cu + NaCl 1:4	61.64	57.79

The porosity measured by Archimedes is different from that of the micro-CT images. The differences could be accounted for; by the nature of the measurement. Over estimation of structures resulted to the porosity and limited resolution of the micro-CT images, which affected the porosities of the measurement.

4.8 Modeling Using Object-Oriented Finite Element (OOF)

OOF2 version 2.1.9 was used in this study. The image must be converted to a portable pixel map format, ppm, from their original formats (jpeg, TIFF.) to be recognizable by ppm2oof. Then assigning properties to each contrast level and meshing the entire image process the image. The second program for computation of mechanical properties uses this processed image.

OOF2 can be used to determine macroscopic properties from images of real microstructures. For this study, the binary images generated using SEM images taken were

taken into consideration in the finite element analysis. First, a pixel groups were generated in OOF2 on the basis of color representing porosity. Then a finite element mesh was generated on the basis of features and colors present in the image by using an adaptive meshing procedure. The two constituents were then assigned material properties, according to the pixel groups defined in the binary image. Figure 32 shows a part of the mesh generated by OOF2 using one of the SEM images for samples. The pixels selected 24018 elements and 15108 nodes and total mesh had approximately 416453 of 2530480
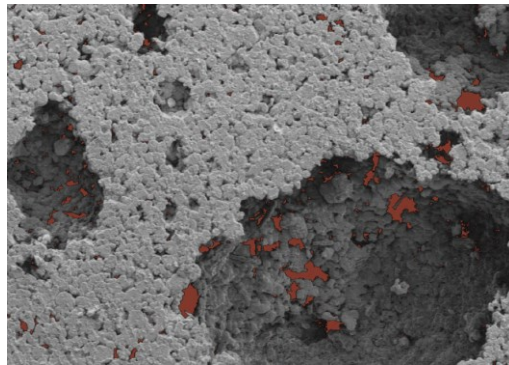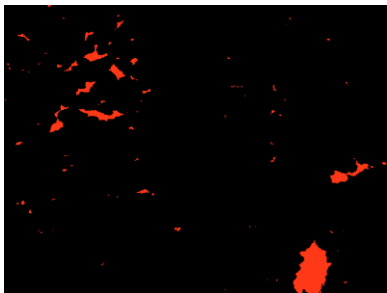
a)
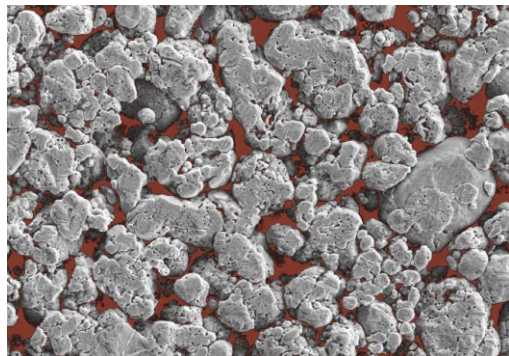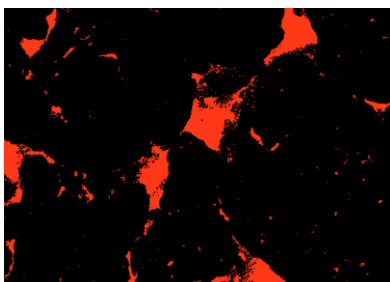
b)
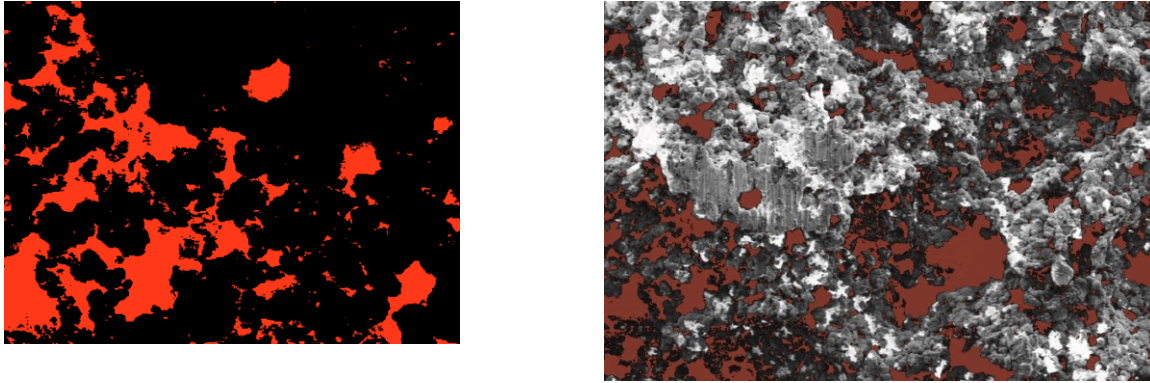
c)
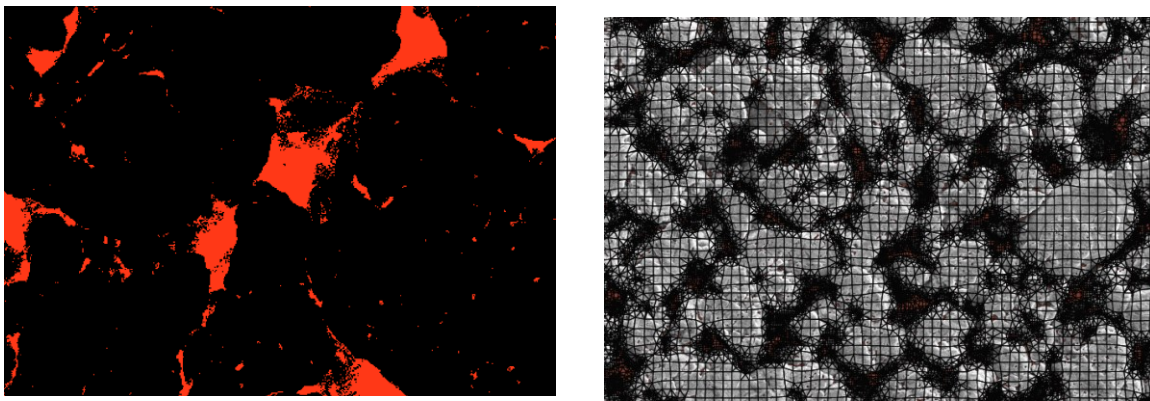
d)

Figure 33. (a-d) the image taken using SEM, which was used to produce micro-and macro porous image.

The OOF model shows the micro and macro pores of porous copper in Figure 31. The results of OOF indicate that can it be used as a powerful tool to predict and derive microstructure and thermal property correlations. The red color represented macro and micro porosity in figure 32. A part of the finite element mesh generated by OOF2 from image. Red area denotes 'Data gray'. For this microstructure, the parameters used were maxscale = 30 pixels, minscale = 10 pixels and threshold = 0.9. The resulting mesh is overlaid on the microstructure in Figure 33d).

CHAPTER 5

Discussion and Future Research

In summary, the production of porous copper samples using space dissolution sintering technique and powder metallurgy route using three different spacer materials (Sodium chloride, Sodium carbonate and potassium carbonate) were successfully accomplished. Micro and macro pores in the range of -500μm for macro pores and less than 100μm for micro pores were obtained through this technique. The maximum porosity value of the porous copper is 66% which is nearly 0.25volume fraction of copper using potassium carbonate as space holder.

The sintering process could be used to achieve smaller pores which is less than 75μm and the larger pores by the space holder removal; it depends on the size, shape and distribution of the space holder particles. Two important problems were encountered when K_2CO_3 was used as space holder. First problem occurred during mixing stage as a result of the shape difference of the copper and K_2CO_3, selective phase separation was observed between copper and Na_2CO_3 powders. Secondly, the appearance of spacer came up after the dissolution process due to of partially texture in the cross section of the samples. When Na_2CO_3 was used, there was a sample weight reduction after second dissolution process and therefore higher dissolution values were found. From this result one can conclude that the Na_2CO_3 particles dissolved faster than NaCl particles at the same sintering and dissolving process.

Table 5 shows that the porosity calculated from density measured by Archimedes is different than porosity observed and then calculated from the micro-CT images. These differences could be accounted for by the nature of each measurement. Archimedes is a weight and volume direct measure and then Equation 3 is used to calculate porosity. In the Nano CT method choosing the right bandwidth between the two selected lines on the color spectrum of the

model was the key to assess the porosity. Errors or misjudgment in selecting the band size can affect the measured porosity. Overestimation of structures and limited resolution of the micro-CT images can all affect the porosity measurement and a standard needs to be developed.

We have described a set of 2D mesh adaptation routines available in the software package OOF2. These routines can be combined into a close to automatic mesh generator, where the input consists of a segmented image, an upper size scale, a lower size scale, and a homogeneity threshold.

Recommendations and Future Work

This research focused on some of the physical properties and mechanical properties of porous copper, other mechanical properties such as fracture toughness, fatigue can also be conducted to achieve a better understanding on how these samples behave in a some certain applications.

Other volume ratios such as 2:1, 3:1 and 4:1 of copper to NaCl, Na_2CO_3 and K_2CO_3 can also be considered in conjunction with varying applied pressures as part of future work. There is also a need for more samples to be created to verify results and for statistics to be performed.

The amount of energy absorbed can also be computed from the plot. Thermal and electrical characterizations of porous metal (copper) can be run and then compared with the results with the OOF, Abaqus and Ansys analysis. Future work may include comparing the quality of elements generated using OOF2 with that of other methods. Work extending the 2D mesh adaptation routines to 3D meshes is also in progress.

References

A. K. Shaik Dawood, S. S. Mohamed Nazirudeen (2010). A Development of Technology for Making Porous Metal Foams Castings. Jordan Journal of Mechanical and Industrial Engineering, 4, 292-299

Andreas Ochsner, Christian Augustin. (2009). Multifunctional Metallic Hollow Sphere Structures. Springer.

Andreas Ochsner, Seyed Mohammad, Hossein Hosseini, Markus Merkel. (2010). Numerical Simulation of the Mechanical Properties of Sintered and Bonded Perforated Hollow Sphere Structures (PHSS). Elsevier, 730-736.

Azarmi, F., Coyle, T., & Mostaghimi, J. (2009). Young's modulus measurement and study of the relationship between mechanical properties and microstructure of air plasma sprayed alloy 625. Surface and Coatings Technology, 203(8), 1045-1054. doi: 10.1016/j.surfcoat.2008.09.035

Bakshi, Srinivasa R., Bhargava, Akanksha, Mohammadizadeh, Seyedreza, Agarwal, Arvind, & Tsukanov, Igor. (2011). Computational estimation of elastic properties of spark plasma sintered TaC by meshfree and finite element methods. Computational Materials Science, 50(9), 2615-2620. doi: 10.1016/j.commatsci.2011.04.003

Bakshi, Srinivasa R., Patel, Riken R., & Agarwal, Arvind. (2010). Thermal conductivity of carbon nanotube reinforced aluminum composites: A multi-scale study using object oriented finite element method. Computational Materials Science, 50(2), 419-428. doi: 10.1016/j.commatsci.2010.08.034

Banhart, J., & Baumeister, J. (1999, 1998). Production methods for metallic foams.

Banhart, John. (2001). Manufacture, characterisation and application of cellular metals and metal foams. Progress in Materials Science, 46(6), 559-632. doi: 10.1016/S0079-6425(00)00002-5

C.E. Wen, M. Mabuchi, Y. Yamada, K. Shimojima, Y. Chino, T. Asahina. (2001). Processing of biocompatible porous Ti and Mg. Elsevier Science Ltd, 1147-1153.

Cady, C. M., Gray, G. T., Liu, C., Lovato, M. L., & Mukai, T. (2009). Compressive properties of a closed-cell aluminum foam as a function of strain rate and temperature. Materials Science & Engineering A, 525(1), 1-6. doi: 10.1016/j.msea.2009.07.007

Castro, Gerhard. (2013). Metallic Syntactic Foams Synthesis, Characterization and Mechanical Properties. (Doctor of Philosophy), Unversity of Southren California

Catrin Kammer, Goslar, Germany. (1999). Aluminium foam. EAA − European Aluminium Association.

da Costa, F. A., da Silva, A. G. P., Ambrozio Filho, F., & Gomes, U. U. (2008). Solid state sintering of a W−25 wt% Ag powder prepared by high energy milling. International Journal of Refractory Metals and Hard Materials, 26(4), 318-323. doi: 10.1016/j.ijrmhm.2007.08.003

Dong, Y., Bhattacharyya, D., & Hunter, P. (2008). Experimental characterisation and object-oriented finite element modelling of polypropylene/organoclay nanocomposites. Composites Science and Technology, 68(14), 2864-2875. doi: 10.1016/j.compscitech.2007.10.026

Duarte, I., & Banhart, J. (2000). A study of aluminium foam formation—kinetics and microstructure. Acta Materialia, 48(9), 2349-2362. doi: 10.1016/S1359-6454(00)00020-3

Ejlali, Azadeh, Ejlali, Arash, Hooman, Kamel, & Gurgenci, Hal. (2009). Application of high porosity metal foams as air-cooled heat exchangers to high heat load removal systems. International Communications in Heat and Mass Transfer, 36(7), 674-679. doi: 10.1016/j.icheatmasstransfer.2009.03.001

Esen, Z., & Bor, Ş. (2007). Processing of titanium foams using magnesium spacer particles. Scripta Materialia, 56(5), 341-344. doi: 10.1016/j.scriptamat.2006.11.010

German, Randall M. (1996). Sintering theory and practice. New York: Wiley.

German, Randall M. (1998). Powder metallurgy of iron and steel. New York: Wiley.

Ivensen, V. A. (1973). Densification of metal powders during sintering. New York: Consultants Bureau.

J. Banhart, H.-W. Seeliger. (2009). Recent Trends in Aluminium Foam Sandwich Technology. Advanced Engineering Materials – Euromat Montpellier.

Jacobs, J. J., Gilbert, J. L., & Urban, R. M. (1998). Corrosion of metal orthopaedic implants. The Journal of bone and joint surgery. American volume, 80(2), 268.

Kashef, Sadaf, Asgari, Alireza, Hilditch, Timothy B., Yan, Wenyi, Goel, Vijay K., & Hodgson, Peter D. (2011). Fatigue crack growth behavior of titanium foams for medical applications. Materials Science and Engineering: A, 528(3), 1602-1607. doi: 10.1016/j.msea.2010.11.024

Lefebvre, L. P., Banhart, J., & Dunand, D. C. (2008). Porous Metals and Metallic Foams: Current Status and Recent Developments. Advanced Engineering Materials, 10(9), 775-787. doi: 10.1002/adem.200800241

Mansourighasri, Amirhossein, Muhamad, N., & Sulong, A. B. (2012). Processing titanium foams using tapioca starch as a space holder. Journal of Materials Processing Technology, 212(1), 83-89. doi: 10.1016/j.jmatprotec.2011.08.008

Mostafid, Ali M. (2007). Entrance and Exit Effects on Flow through Metallic Foams. (Degree of Master), Concordia University, Canada.

N. Babcsán , J. Banhart , D. Leitlmeier. (2003). METAL FOAMS – MANUFACTURE AND PHYSICS OF FOAMING. ADVANCED METALLIC MATERIALS.

Narayan, Roger, & SpringerLink. (2009). Biomedical Materials. Boston, MA: Springer US.

Ryan, G., Pandit, A., & Apatsidis, D. P. (2006). Fabrication methods of porous metals for use in orthopaedic applications. Biomaterials, 27(13), 2651-2670. doi: 10.1016/j.biomaterials.2005.12.002

Schueren, B. Van der, & Kruth, J. P. (1995). Powder deposition in selective metal powder sintering. Rapid Prototyping Journal, 1(3), 23-31. doi: 10.1108/13552549510094241

Shapovalov, Vladimir I. (2002). Prospective Manufacture and Aircraft Applications of cast Metal Porous Materials. Sandia National Laboratories.

Sharma, M., Gupta, G. K., Modi, O. P., Prasad, B. K., & Gupta, Anil K. (2011). Titanium foam through powder metallurgy route using acicular urea particles as space holder. Materials Letters, 65(21-22), 3199-3201. doi: 10.1016/j.matlet.2011.07.004

Shehata Aly, Mohamed, Almajid, Abdulhakim, Nakano, Satoshi, & Ochiai, Shojiro. (2009). Fracture of open cell copper foams under tension. Materials Science & Engineering A, 519(1), 211-213. doi: 10.1016/j.msea.2009.04.062

Shih, Albert J., & Huang, Zhenhua. (2006). Three-Dimensional Optical Measurements of Porous Foams. Journal of Manufacturing Science and Engineering, 128(4), 951. doi: 10.1115/1.2194556

Singh, R., Lee, P. D., Lindley, T. C., Dashwood, R. J., Ferrie, E., & Imwinkelried, T. (2009). Characterization of the structure and permeability of titanium foams for spinal fusion devices. Acta Biomater, 5(1), 477-487. doi: 10.1016/j.actbio.2008.06.014

Smorygo, O., Marukovich, A., Mikutski, V., Gokhale, A. A., Reddy, G. Jagan, & Kumar, J. Vinod. (2012). High-porosity titanium foams by powder coated space holder compaction method. Materials Letters, 83, 17-19. doi: 10.1016/j.matlet.2012.05.082

Surace, R., De Filippis, L. A. C., Ludovico, A. D., & Boghetich, G. (2009). Influence of processing parameters on aluminium foam produced by space holder technique. Materials & Design, 30(6), 1878-1885. doi: 10.1016/j.matdes.2008.09.027

Tamayol, A., & Hooman, K. (2011). Thermal assessment of forced convection through metal foam heat exchangers. Journal of Heat Transfer, 133(11), 111801.

Tano, Ingrid. (2012). Contributions to Multivariate Process Capability Indices. (PhD), Luleå University of Technology, Sweden.

Thabarealam, Tharikalam. (2009). Production, Processing and Characterisation of Porous TiAl Alloy Produced Using Space Holder Method. (Masters of Engineering), University of Waikato.

W.S. Sanders, L.J. Gibson (2003). Mechanics of hollow sphere foams. Materials Science and Engineering, 70-85.

Wang, Lin Biao, See, Kye Yak, Ling, Yong, & Koh, Wee Jin. (2012). Study of metal foams for architectural electromagnetic shielding. Journal of Materials in Civil Engineering, 24(4), 488-493. doi: 10.1061/(ASCE)MT.1943-5533.0000403

Appendix

OOF2 Tutorial Guide

It's a good idea to read through this tutorial before you venture into more task- specific ones, just to make yourself familiar with various OOF2 parts. To go to the next tutorial page, click on the Next button below. Sometimes the Next button will be grayed out this means that you have to perform the action described in the tutorial page before proceeding. The Back button below will take you to the previous tutorial page. The Jump button takes you to the highest numbered page that you've visited in this session.

Use the Save button to save a tutorial session in a file so that you can resume it later. To resume a session, load the saved file with the Load Script command in the File menu in the main OOF2 window. OOF2 creates and manipulates a variety of data structures ("objects", in the lingo), which are described here briefly so that they can be referred to later in the tutorials.

Microstructure: A grid of pixels with Materials assigned to them. Microstructures have a fixed height and width in physical units. Microstructures also contain other data structures, defined below.

Image: Just what it sounds like a grid of pixels with colors assigned to them. Every Image in OOF2 is assigned to a Microstructure. The Image and the Microstructure must have the same size. A Microstructure can have many Images assigned to it.

Material: A collection of Properties, which define the physical behavior of the material at a point in a Microstructure.

Property: Something that contributes somehow to the definition of a material. Some Properties correspond directly to terms in a constitutive equation (eg, elasticity, thermal conductivity), and some contribute indirectly (eg, orientation). They can also be purely decorative (e.g. color).

Skeleton: The geometry of a finite element mesh, specifying where the nodes, edges, and elements are, but without any further information. Skeletons are created within Microstructures. A single Microstructure can contain many Skeletons.

Mesh: A full finite element mesh, including information about element type, which fields are defined, which equations are being solved, boundary conditions, etc.

Subproblem: A part of a finite element mesh. A mesh can contain many subproblems. Subproblems can differ in the mesh elements included in them, in the fields defined on them, or the equations solved on them. When a Mesh is created, a default Subproblem that includes all Mesh elements is created automatically.

OOF2 has no preferred set of units. Enter data in any set of units that you prefer, and the output will be in those units. Of course, at NIST we prefer that you use SI units (kilograms, meters, and seconds, etc.), but if you use slugs, furlongs, and fortnights instead, OOF2 will not complain.

A Sample Example

This tutorial is designed to familiarize users with OOF2 by guiding them through a simple but complete project.

We assume that you run this tutorial from a fresh start of OOF2. Whether you run it this way or not don't make any significant difference but it simplifies things in a few places.

Objective: A simple finite element analysis of a fictitious microstructure under uniaxial tension. The microstructure is composed of two fictitious materials named yellow and cyan with linear elastic properties given by:

Yellow: E=1.0, nu=0.3

Cyan: E=0.5. nu=0.3
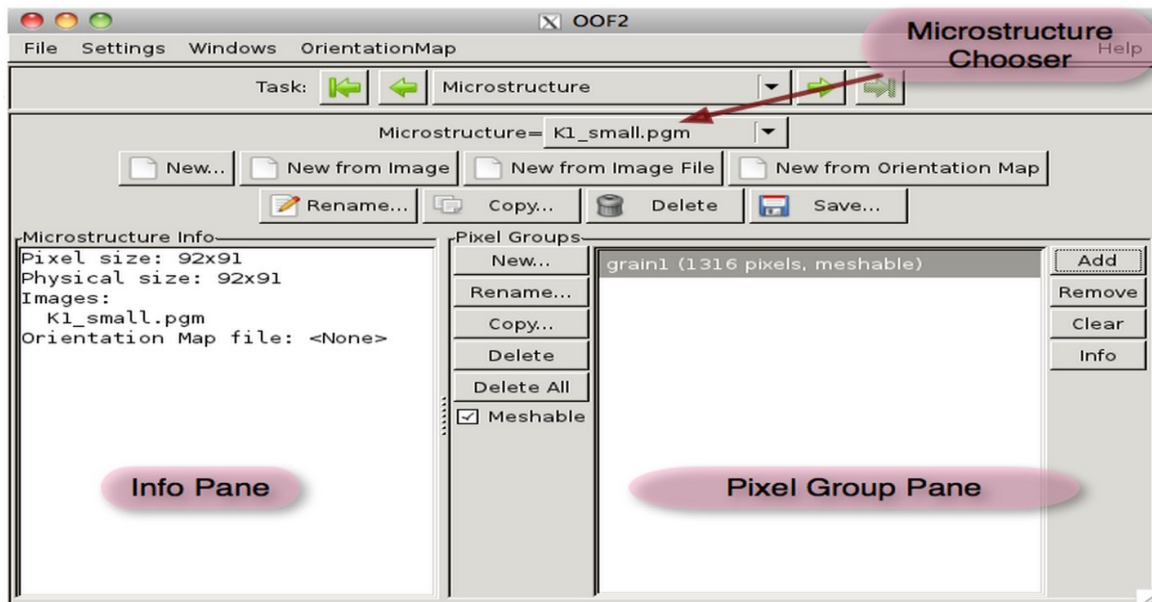
Open a graphics window, if none has been opened yet, with the Graphics/New command in the Windows menu in any OOF2 window.

Locate the file cyallow.png within the share/oof2/examples directory in your OOF2 installation.
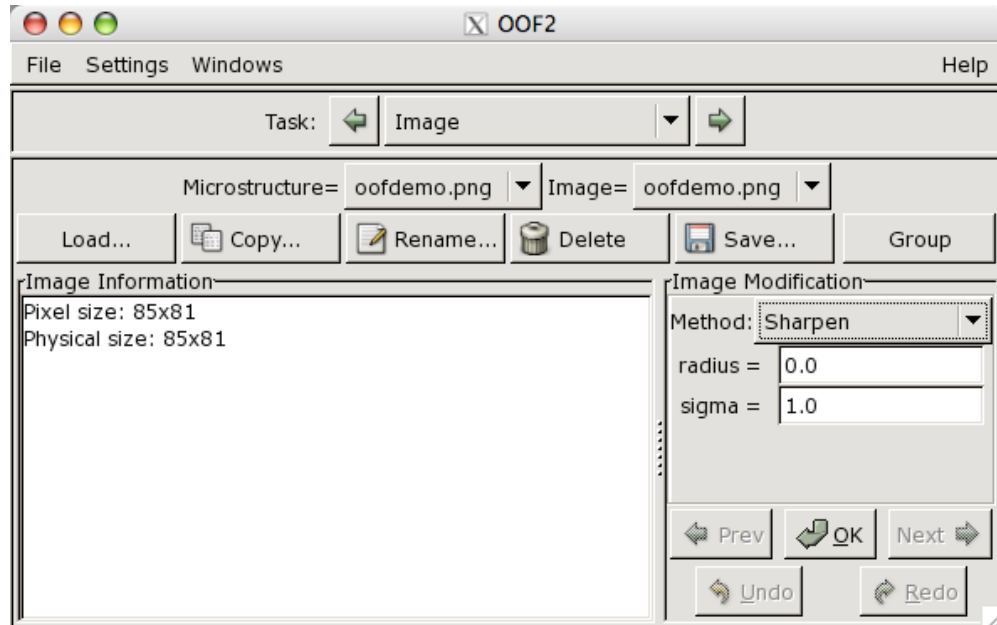
Open the Microstructure page from the Task menu in the main OOF2 window.

Create a new Microstructure from an existing image file by clicking the New from Image File button.

In the file selector, navigate to cyallow.png. For now, leave the microstructure_name, width and height values set to automatic. Click OK.

Open the Image page in the main OOF2 window.

The Group button, and click OK in the dialog box.

Go back to the Microstructure page, and notice that two pixel groups have been created. The automatically generated names of the pixel groups are not terribly convenient. The groups can be renamed.

Select the first pixel group, RGBColor (red=1.00, green=1.00, blue= ....).

Once it's been highlighted, click Rename.

Delete the old name and type in yellow, which is the actual color of the group. (Triple-clicking on the old name in the dialog box will select the whole name, making it easier to replace.)
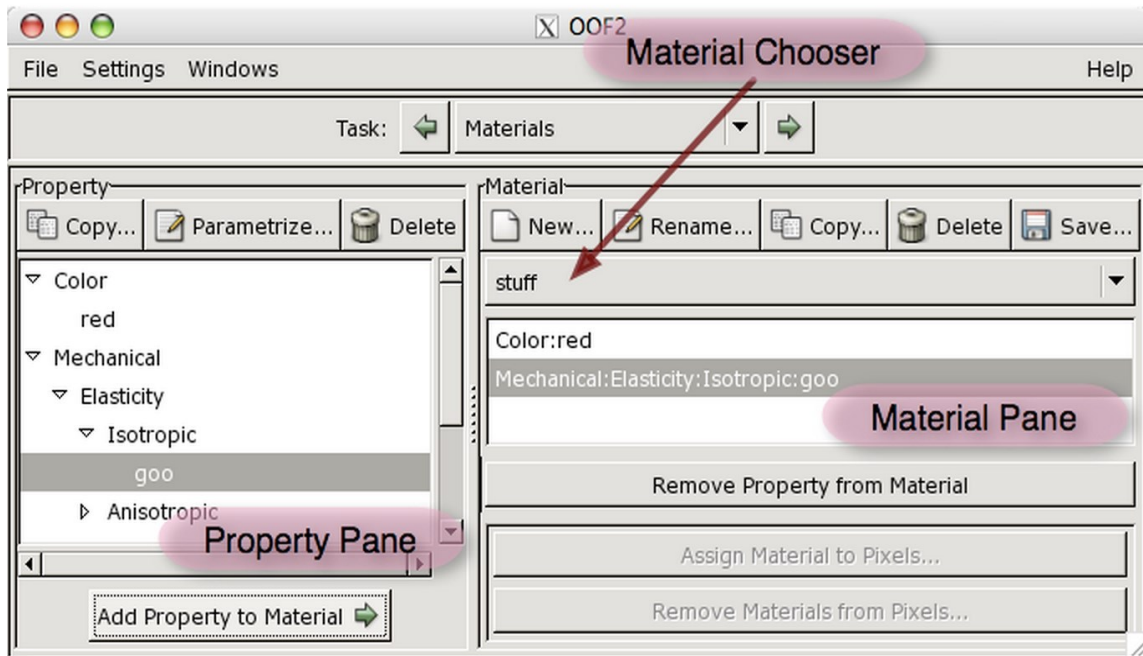
Click OK to finalize the change.

Select the second pixel group and Rename it to cyan.

Now you're ready to create materials for each pixel group.

Open the Materials page in the main OOF2 window.

Click OK.

Create a second New material with the name cyan-material.

We now need to make materials meaningful by adding properties to them.

Start creating a property for yellow-material by selecting Isotropic from Elasticity in the Mechanical property hierarchy.

Click Copy and check the box to give it a user-defined name. (Use the Copy button in the Property pane, not the one in the Material pane!)

Type in yellow_elasticity and click OK.

Select yellow_elasticity from the Property hierarchy and either double click it or click the Parametrize... button to input actual values.

The elasticity parameters can be entered in a variety of formats. The default format is Cij. Change it to E and nu with the pull down menu at the top of the Parametrize dialog box.

Set the Young's modulus (young) to 1.0 and Poisson's ratio (Poisson) to 0.3.

Click OK to finish up.

Below the New button in the Material pane is a pull-down menu that lists all of the Materials that have been defined. Select the yellow-material that you defined earlier.

Make sure that the yellow_elasticity Property is still selected.

Click Add Property to Material in the Property pane to add the Property to the Material.

Make another Copy of Isotropic and name it cyan_elasticity. Parametrize the property cyan_elasticity with these values: young=0.5, poisson=0.3. Select cyan-material in the Material selector in the Material pane, and add the Property cyan_elasticity by clicking on the Add Property to Material button.

Select a Property in the Material pane and use the Remove Property from Material button if you've made a mistake.

Copy the Color property in the Property pane, giving the copy the name yellow.

Parameterize the yellow Property. In the Parameterize dialog box, switch from GrayColor to RGBColor, and set the Red, Green, and Blue sliders to something yellowish, say Red=1, Green=0.8, and Blue=0. Click OK.

Add the yellow Property to the yellow-material.

Similarly create a Color property for cyan and add it to the cyan-material. Parameterize it with Red=0, Green=0.8, and Blue=1.

Now that we have defined Materials and created pixel groups in the Microstructure, we can assign Materials to the microstructure.

Select the material yellow-material and click on the button labelled Assign Material to Pixels... in the Material pane. The pop-up window lets you choose the Microstructure to which the Material will be assigned (currently we only have one, "cyallow.png"), and the pixels within the

Microstructure. Choose the pixel group yellow in the pixels pull-down menu. Click OK to finish.

The graphics window displays many things automatically, but if you want to view a Microstructure you must tell it to do so explicitly by adding a new Display Layer.

Dig up the Graphics window that you opened earlier by choosing Graphics/Graphics 1 in the Windows menu on any OOF2 window.
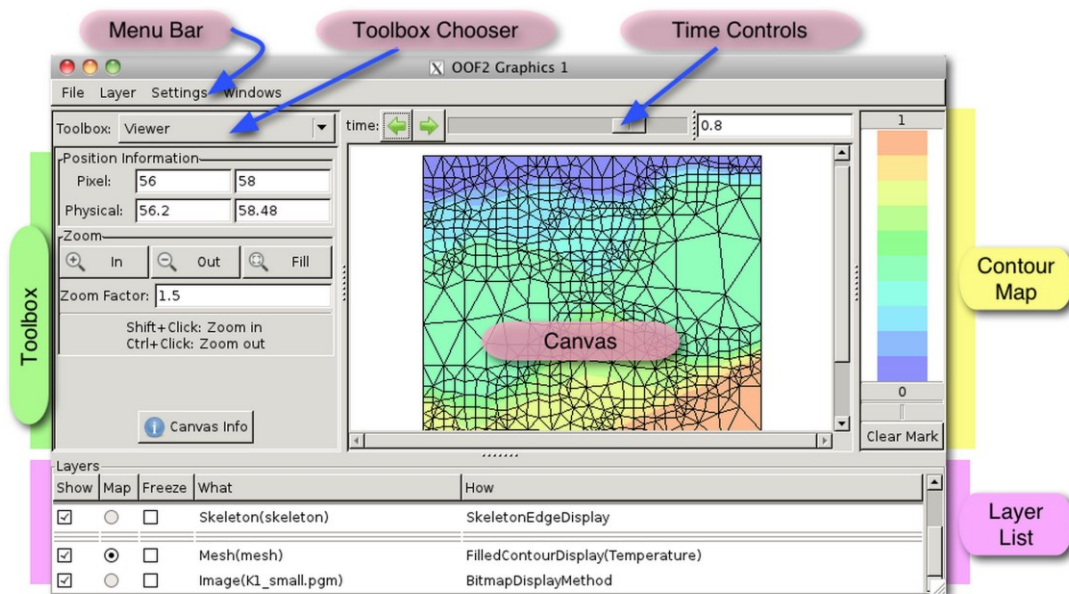
Select New from the Layer menu in the Graphics window.

Choose Microstructure in the category pull-down menu. Since you have defined only one Microstructure, "cyallow.png", it's shown in the object menu.

An object being displayed may appear in more than one Layer. The layers for the object selected in the Displayed Object pane on the left side of the Layer Editor are listed in the Display Methods list on the right side.

Click the New button below the Display Methods list. Click the OK button.

Select the cyan-material in the Material pane in the main OOF2 window and assign it to the pixel group named cyan.

One Skeleton can be used to create many different meshes, with different element types and different physical fields.

Open the Skeleton page in the main OOF2 window.
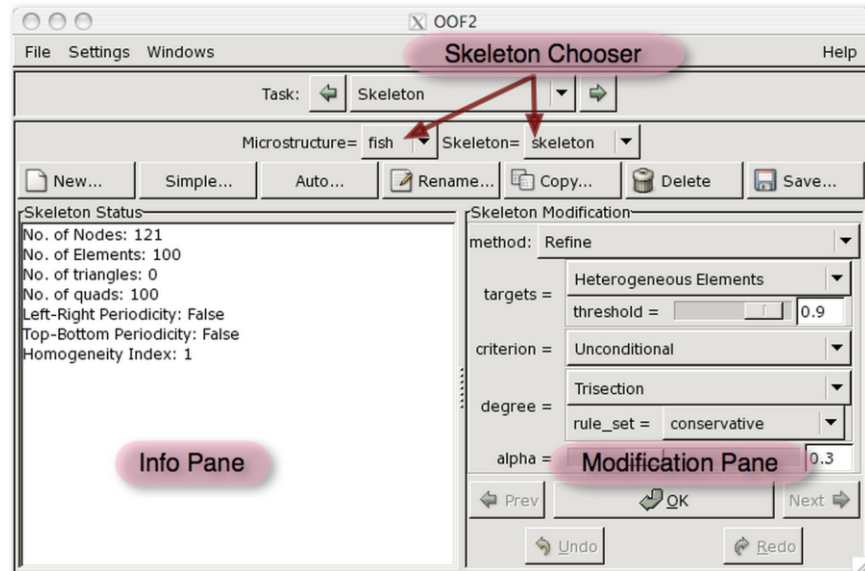
Click the New button to open up a skeleton initializer. To keep things simple, just click OK to create a 4x4 grid of quadrilateral skeleton elements.

The Skeleton is now displayed on top of the Microstructure in the graphics window.

Click on the chooser widget for the method parameter in the Skeleton Modification pane and select Snap Nodes.

Set alpha to 1.0. Place the mouse over the labels and menu items to see an explanation of what the parameters mean.

Click OK to modify the skeleton.

All the elements in the skeleton are now completely homogeneous.

It's time to create an FE mesh based on this skeleton.

Open the FE Mesh page.
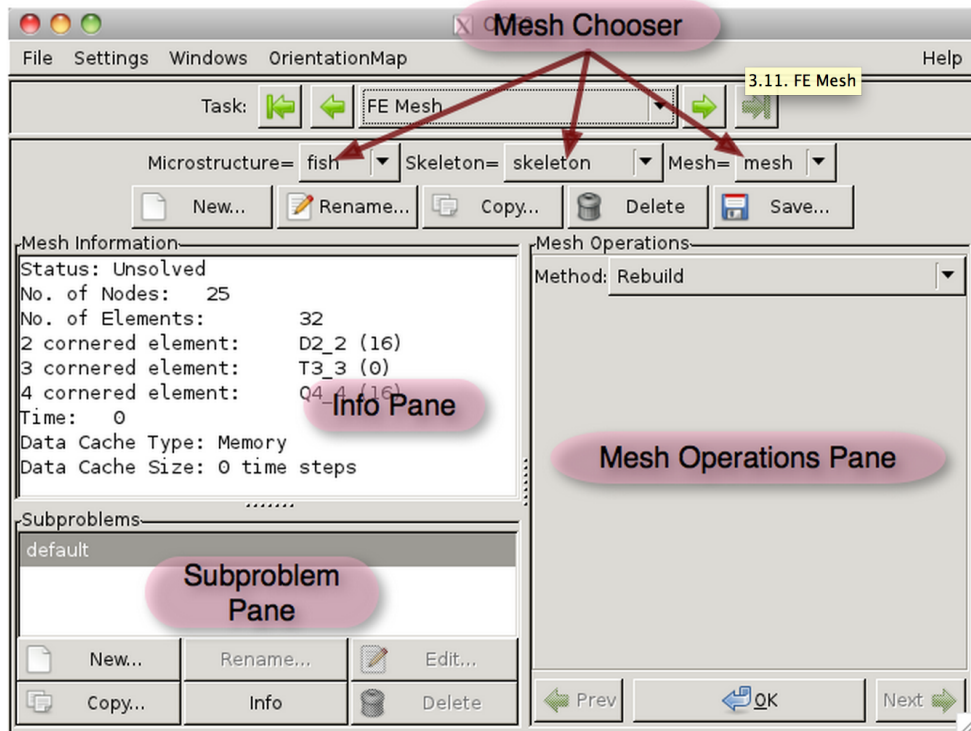
Click the New button to get a dialog box for creating a new Mesh.

The pull-down menus labeled 2-cornered element, 3-cornered element and 4-cornered element list the available element types that are consistent with the polynomial orders chosen. There's only one choice for each: D2_2, T3_3 and Q4_4. Positioning the mouse over the menus will bring up a tooltip describing the element type.

Click OK to create an FE Mesh.

Proceed to the Fields & Equations page.
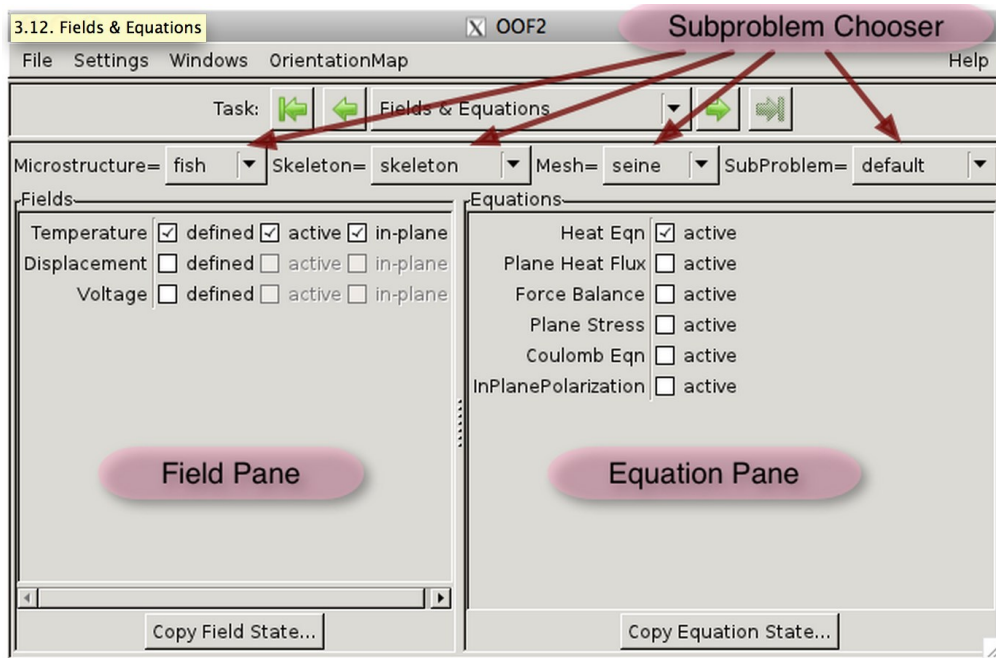
Here, we need to tell OOF2 about the (known) unknowns of the problem that we're trying to solve. Fields are defined if they have been given values on the Mesh.

Fields are active if the solver will find their values. Only defined fields can be active.

Fields are in-plane if they have no out-of-plane derivatives. (This is a generalization of plane-strain.)

We're solving a uniaxial tension problem, so displacement is the only (known) unknown.

Check all three boxes for the Displacement field.

We're solving the Force_Balance equation, so check the corresponding box on the right hand side of the Fields & Equations page.

Now, move to the Boundary Conditions page.
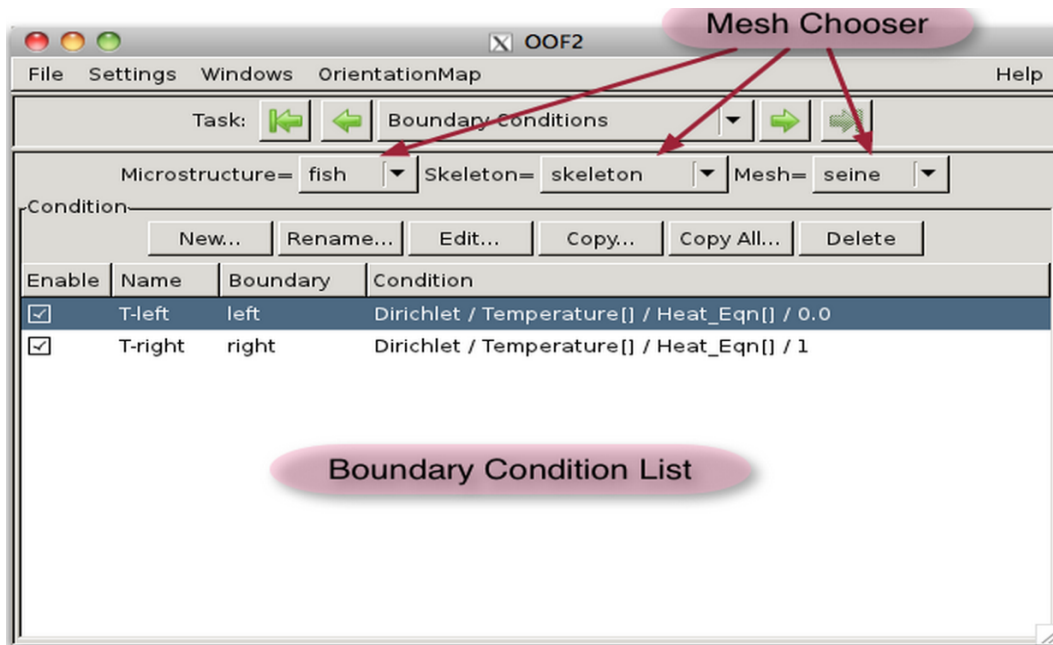
The boundary conditions we're going to apply are:

1. u_x = 0 on the left side

2. u_y = 0 on the bottom side

3. u_x = 10.0 on the right side

The Boundary Condition page has two panes, Profile and Condition. The Profile pane allows you to predefine the functional form of a boundary condition.

Since only one Field is defined and only one Equation is active for this example, the field and equation will have only one choice each, Displacement for field and Force_Balance for equation. Go to the next slide to really set the boundary conditions.

Click the New... button in the Condition pane to bring up a boundary condition builder. Leave it set to Dirichlet boundary conditions, which gives Fields fixed values at the boundaries.

The first B.C. deals with displacement in the x-direction, so select x for both Displacement and Force_Balance components.

The profile is the functional form of the Field along the boundary. The predefined boundaries in OOF2 (top, left, bottom, right) go counterclockwise around the microstructure. Set the profile to Constant Profile with value=0.0.

Finally, choose the boundary to which this condition should be applied (left) and click OK.

Important Note Do not click the Apply button in the builder window.

Click New... to add the second boundary condition.

Select y for both Displacement and Force_Balance components.

Select Constant Profile and type in 0.

This conditions going to be applied to the bottom of the mesh. Select bottom and click OK to finish.

Click New... to add the third boundary condition.

Select x for both Displacement and Force_Balance components.

Its value is 10.0, which is constant along the side. Select Constant Profile and type in 10.0.

This conditions going to be applied to the right side of the mesh. Select right and click OK to finish. We've just finished creating all three boundary conditions.

Open the Solver page. There are three subregions of the page.
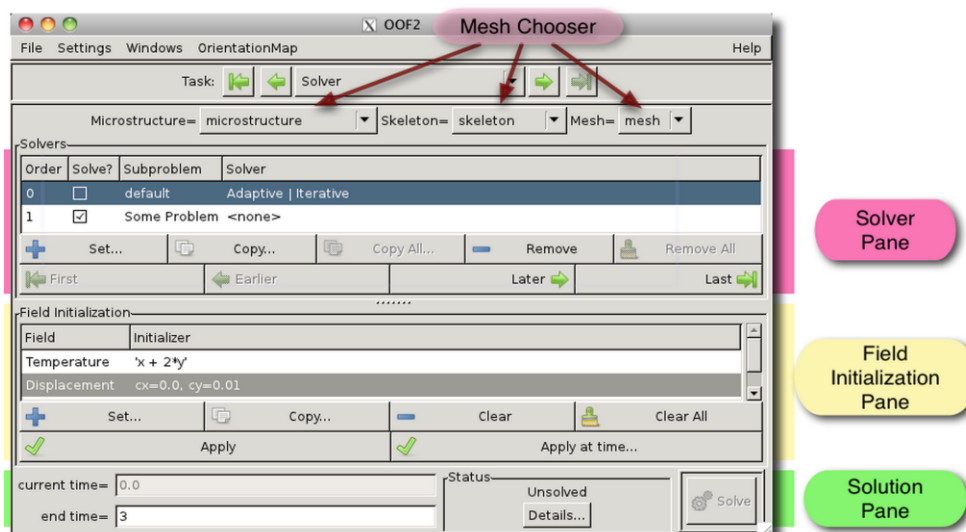
Select the default subproblem in the top pane, and either double click it or click the Set Solver...

button. Just click OK.

We're almost at the end of this tutorial.

ClickSolve